國 立 交 通 大 學

電信工程學系

碩 士 論 文

以集總與分散式元件設計任意功率分配之旁枝耦合器

Analysis and Design of Lumped- and Distributed- Element Branch-Line Coupler with Arbitrary Power Division

研究生：盧政良

指導教授：郭仁財博士

中 華 民 國 九十八 年 七 月

以集總與分散式元件設計任意功率分配之旁枝耦合器

Analysis and Design of Lumped- and Distributed- Element Branch-Line Coupler with Arbitrary Power Division

研究生：盧政良 **Student:Zheng-Liang Lu**

指導教授：郭仁財 博士 **Advisor:Dr. Jen-Tsai Kuo**

國立交通大學

電信工程學系

碩士論文

A Thesis
Submitted to Department of Communication Engineering
College of Electrical and Computer Engineering
National Chiao Tung University
in Partial Fulfillment of the Requirements
for the Degree of
Master of Science
in
Communication Engineering
June 2009
Hsinchu, Taiwan, Republic of China

中華民國九十八年七月

以集總與分散式元件設計任意功率分配之旁枝耦合器

研 究 生：盧 政 良　　指 導 教 授：郭 仁 財　博 士

國立交通大學電信工程學系

摘要

本論文提出分析與設計方式，以集總元件實現具有寬頻、任意功率分配之三級旁枝耦合器。藉由奇偶模分析，可知調整旁枝的傳輸線阻抗控制旁枝耦合器的功率分配。同時，在一定的功率分配下，頻寬的大小可以理論預測。本論文進一步利用集總與分散式元件，以縮小三級旁枝耦合器的面積，並比較純以集總元件實現之電路和集總與分散式元件實現之電路之間的差異。本論文實作兩電路，以驗證本文之設計，量測數據與模擬結果相當一致。

Analysis and Design of Lumped- and Distributed- Element Branch-Line Coupler with Arbitrary Power Division

Student: Zheng-Liang Lu

Advisor: Dr. Jen-Tsai Kuo

Department of Communication Engineering

National Chiao Tung University

Abstract

This thesis designs a 3-section wideband branch-line coupler with an arbitrary power division. Through the even/odd mode analysis, the arbitrary power division can be achieved by controlling the characteristic impedances of the branch lines. Meanwhile, for a specified power division, the fractional bandwidth can be predicted theoretically. The 3-section branch-line couplers are implemented by lumped elements and lumped distributed elements to reduce the circuit size. Theoretical analysis is validated by measurement results of experimental circuits.

誌謝

能順利完成論文首先要感謝指導老師，郭仁財教授。經過老師兩年的辛勤指導，帶領我瞭解微波被動電路的專業知識和技能，同時老師對於做學問的態度和熱情，讓我學習到做人處事應有的本分。此外，感謝口試委員：陳俊雄教授、張志揚教授與林祐生教授，對於學生論文提供珍貴的意見。

感謝父母與家人對我兩年來的支持。感謝佳芊在我身處水深火熱之時溫柔的陪伴。感謝 908 實驗室的各位，實驗室溫馨和樂的氛圍讓我覺得值得依賴。感謝實驗室的大學長逸群在我的研究上幫助甚多，也感謝實驗室同屆伙伴的相互扶持：邊衝浪又可以把研究做得好極了的正修，懂得享受生活又會做研究的評翔，還有愛吃老陳雞排配日劇的秉岳；還有感謝實驗室優秀又可愛的學弟妹：麒宏、紹展、峻瑜、卓諭、宣融、詩薇與祖偉。另外也感謝 912 實驗室的肇堂和 903 實驗室的菡澤，在最後實作階段上的意見交換。謝謝大家。

Table of Contents

List of Figures

List of Tables

Chapter 1
Introduction

The branch-line coupler is one of the most popular hybrids used in microwave and millimeter wave sub-systems such as balanced amplifiers, phase shifters, power dividers, and mixers. In this chapter, the history of its development is presented first. Then, some literatures on size-reduction and wideband design are discussed. Finally, the organization of the thesis is described.

1.1 History

Conventional branch-line coupler was first reported [1] by J. Reed and G. J. Wheeler in 1956. Using the even/odd mode analysis, the four-port network can be reduced to a half circuit such that the analysis is simply a superposition of the two modes. In 1968, Levy [2] proposed a synthesis method for multi-section branch-line coupler using exact Chebyshev and Butterworth characteristics and implemented the circuits by waveguide. In 1985, an optimum design of branch-line coupler using microstrip lines was reported by Y. Naito [3]. Except for using similar design as [2], the realizable impedance range for microstrip line was studied to make the impedance levels of branch-line couplers reasonable, so that circuits can be physically fabricated by microstrip lines.

1.2 Size-Reduction Design

Up to now, branch-line couplers have been implemented using the microstrip line, stripline, coplanar waveguide (CPW), and multilayer structures. However their

sizes are relatively large due to the quarter-wavelength transmission line sections. Thus, the reduction of the size associated with these transmission lines is essential in decreasing the size of the branch-line coupler. Lots of attempts have been contributed to reduce circuit area. Conventionally, these works can be classified into two groups. One is achieved by using the folded line configuration, and the other is accomplished by adopting lumped-element components such as metal-insulator metal (MIM) capacitors.

In 1990, the approach in [4] utilizing combinations of short high-impedance transmission lines and shunt lumped capacitors to design a reduced-length transmission line section can largely miniaturize the branch-line coupler. Based on this, similar ideas have been proposed in [5]-[10]. In [5], a branch-line coupler with eight stubs inside the coupler was proposed for 25% size reduction. In [6] and [7], Hong proposed 2-section and 3-section branch-line couplers with lumped distributed elements, and size-reduction of 35% and 54%, can be achieved respectively. In 2007, Tang [8] proposed a synthesis method utilizing multiple shunt open stubs for miniaturizing the four quarter-wavelength transmission line sections of the conventional branch-line couplers. Authors also concluded that the more open stubs with low impedance utilized, the broader the bandwidth will be. In [9] and [10], T-shape structure of reduced-line and its quasi-lumped elements approach are used to have a size-reduction of 55% and 70%, respectively. Periodic shunt transmission line section with capacitances can be also used to reduce the physical length, as shown in [11].

Based on finite-ground coplanar-waveguide (FGCPW) structures [12], bended structure with adding an external compensation network to improve the bandwidth has been proposed. Branch-line coupler using three-dimensional structure of the low-temperature co-fired ceramic (LTCC) substrate can be available in the MIC and

MMIC applications [13]. In 2008, a dual transmission line equivalent to the conventional transmission line [14] is exploited to miniaturize a branch-line coupler. They demonstrated that this approach can achieve size-reduction to 63.9%. The artificial line approach [15] can also be used to implement couplers with the size reduction.

Lumped-element design methods are used to realize the coupler circuit within a reasonable chip area in various MIC or MMIC applications. In the conventional quadrature design methods, one-section high-pass networks based on the branch-line design technique was proposed by Gupta and Getsinger [16]. The dual form of a two-section quadrature coupler constructed by low-pass networks was designed and analyzed by Vogel [17]. Although the lumped-element quadrature couplers designed by the previous methods achieve a good isolation and voltage standing-wave ratio (VSWR), the amplitude balance between output ports can be maintained only within a narrow bandwidth. To achieve a flat coupling over a wider bandwidth, a hybrid of the lumped- and distributed-element method and a broad-band matching design technique is proposed by Vogel and Ohta, respectively, in [17], [18].

1.3 Wideband Design

Wide-band circuits are now in demand as wide-band systems such as ultra-wideband (UWB) become practical. There are a couple of circuits for broad-band purpose, such as a Lange coupler, tandem coupler, and so on. They show wide-band performances with small sizes, but most of them need multilayered or air-bridged structures for tight coupling and signal routing over a wide frequency range. The branch-line coupler has narrow-band characteristics with a large circuit area. Although there are several solutions to solve the large-size problem mentioned

above, they cannot enhance the bandwidth. In open literature, such as [6]-[7] and [19]-[20], the cascaded branch-line couplers can enlarge the bandwidth. In [6] and [7], Hong also concluded that the bandwidth can be enhanced to be larger than 56%. In [19], Chiang analyzed the 2-section branch-line coupler with lumped elements and demonstrated a fractional bandwidth of 50%. Lumped-element quadrature hybrids consisting of two-section inductively coupled networks have also been developed to realize the proposed hybrid with very good balance in both magnitude and phase between the output ports over a fractional bandwidth of 38% [20].

In this thesis, analysis and design for a 3-section branch-line coupler with arbitrary power division is described. Through the control of the characteristic impedance of one branch, the design is not only for arbitrary power division but also specified for desired fractional bandwidth. Due to the large size, in Chapter 3, the equivalent circuits of multi-section T and π model with lumped elements are under study for miniaturization. In consideration of implementation in MIC and MMIC applications, the proposed circuits are miniaturized by lumped- and distributed elements with simulation and measurement. Chapter 4 draws the conclusion.

Chapter 2

Design of 3-Section Branch-Line Coupler with Arbitrary Power Division

In this chapter, the conventional branch-line coupler and 2-section branch-line coupler presented is reviewed. In section 2, 3-section branch-line coupler with arbitrary power division is studied and simulations are demonstrated to confirm the idea.

2.1 Reviews on Branch-Line Couplers

Branch-line coupler is one of quadrature couplers with phase difference of 90^0 in the outputs of the through and coupled ports. The branch-line coupler has a high degree of symmetry, since any port can be used as the input port. The output ports are on the opposite side of the junction from the input one, and the isolation port is the remaining port on the same side as the input port. Using even/odd mode analysis, the scattering matrix can be derived and it reflects the symmetry [21].

2.1.1 Conventional Branch-Line Coupler

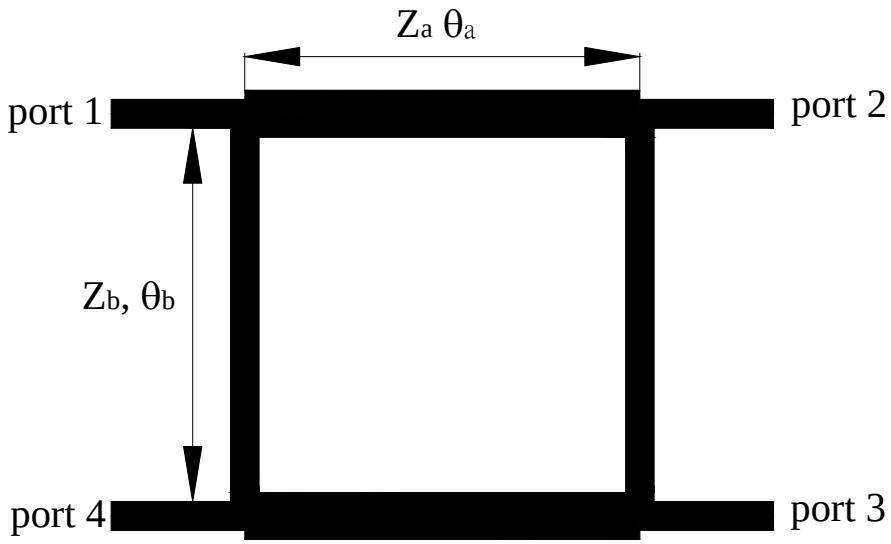

Fig. 2-1. Conventional branch-line coupler

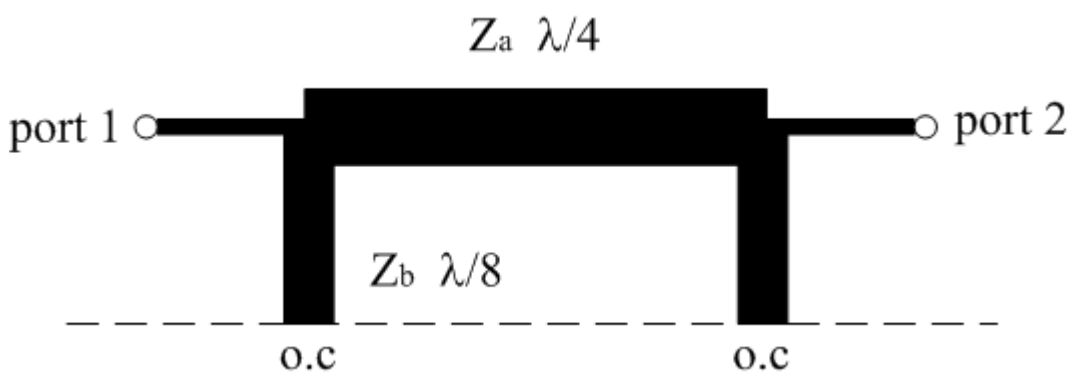

(a)

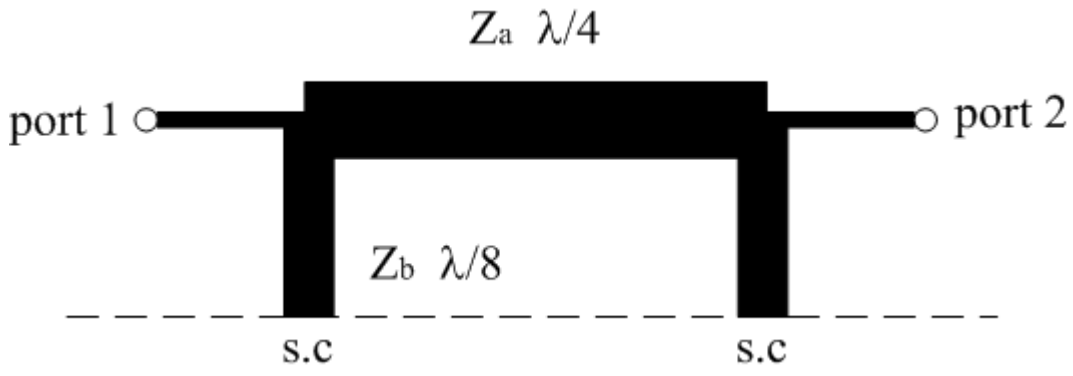

(b)

Fig. 2-2. Even/odd mode analysis of the circuit in Fig. 2-1. (a) Even mode (b) Odd mode

Fig. 2-1 shows the layout of conventional branch-line coupler. The reference impedances for the four ports are 50 ohm. All the sections are quarter-wavelength at the central frequency with characteristic impedances Z_a and Z_b. Signal propagates along with main line to port 2 (through), and part of signal further continues along with the branch to port 3 (coupling). Port 4 is isolated since the phase difference between two channels is 180 degrees, and then the deconstructive interference occurs. The control of coupling level subject to characteristic impedance of the branch will be demonstrated.

Even/odd mode analysis of the circuit is used to derive the S parameters. The circuits reduced with respect to the symmetric plane are shown in Fig. 2-2 (a) and (b). The ABCD matrices of the even and odd modes are:

$$ABCD_{even} = \begin{bmatrix} -z_a y_b & jz_a \\ jz_a\left(y_a^{\,2} - y_b^{\,2}\right) & A_e \end{bmatrix} \tag{2.1}$$

$$ABCD_{odd} = \begin{bmatrix} -A_e & B_e \\ C_e & -A_e \end{bmatrix} \tag{2.2}$$

where $z_a = \dfrac{Z_a}{Z_0}$ and $y_b = \dfrac{Z_0}{Z_b}$, with $Z_0 = 50\ \Omega$.

The conversion between S parameters and ABCD parameters can be written as:

$$S_{11} = \frac{\Gamma_e + \Gamma_o}{2} \tag{2.3a}$$

$$S_{21} = \frac{\tau_e + \tau_o}{2} \tag{2.3b}$$

$$S_{31} = \frac{\tau_e - \tau_o}{2} \tag{2.3c}$$

$$S_{41} = \frac{\Gamma_e - \Gamma_o}{2} \tag{2.3d}$$

where $\Gamma_{e/o} = \left(\frac{A+B-C-D}{A+B-C-D} \right)_{e/o}$ and $\tau_{e/o} = \left(\frac{2}{A+B-C-D} \right)_{e/o}$. When input is excited at port 1, for instance, $S_{11} = S_{41} = 0$ at the design frequency should be enforced. Based on these conditions, the S matrix for a branch-line coupler can be derived as follows:

$$[S] = \frac{-1}{\sqrt{1+z_b^{\,2}}} \begin{bmatrix} 0 & jz_b & 1 & 0 \\ jz_b & 0 & 0 & 1 \\ 1 & 0 & 0 & jz_b \\ 0 & 1 & jz_b & 0 \end{bmatrix} \tag{2.4}$$

The diagonal terms in (2.4) vanish for input matching at central frequency, and $S_{41} = S_{14} = S_{23} = S_{32} = 0$ for isolation purpose. The ratio $\frac{S_{21}}{S_{31}} = jz_b$ stands for power division $z_b^{\,2}:1$ and the phase of through port leading over coupling port. Typically, the fractional bandwidth is about 15% ~ 20%. The circuit size is $\frac{\lambda^2}{16}$.

2.1.2 2-Section Branch-Line Coupler

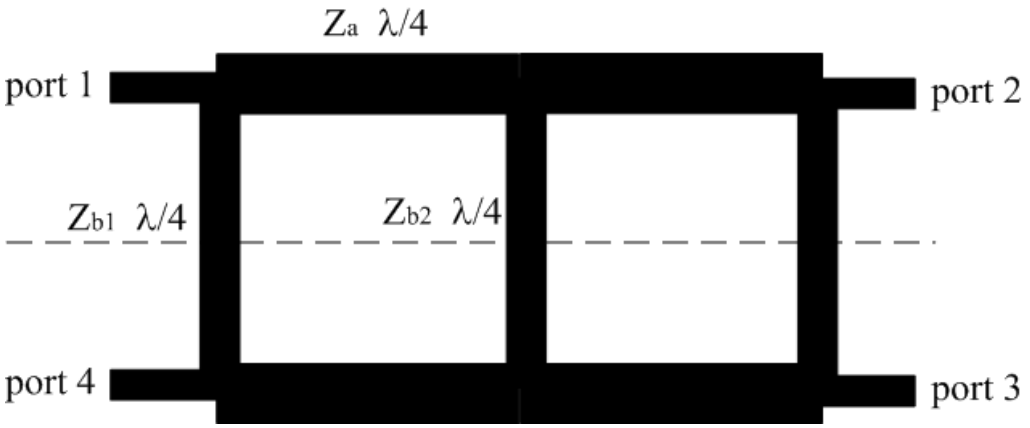

Fig. 2-3. A 2-section branch-line coupler.

Multi-section branch-line coupler can be used to enhance the fractional bandwidth. Fig. 2-3 shows the 2-section branch-line coupler. The analysis procedure is the same as one in previous section. Herein, the design formulas are listed as follows for reference:

$$c = |S_{31}| = \frac{2y_B^{\,2}}{1 - y_B^{\,2}} \tag{2.5}$$

$$Z_{B1} = Z_0 \frac{c}{1 - \sqrt{1 - c^2}} \tag{2.6}$$

$$Z_{B2} = Z_0 \frac{z_A^{\,2}}{c} \tag{2.7}$$

where Z_0 is the reference impedance, z_A for normalized impedance and c is coupling. Note that z_A typically ranges between 0.6 and 3 if Z_0 = 50 ohm. The circuit size is about $\frac{\lambda^2}{8}$ at the design frequency. It is worth noting that the 2-section branch-line coupler possesses a fractional bandwidth about 30%.

2.2 3-Section Branch-Line Coupler

2.2.1 Even/Odd Mode Analysis

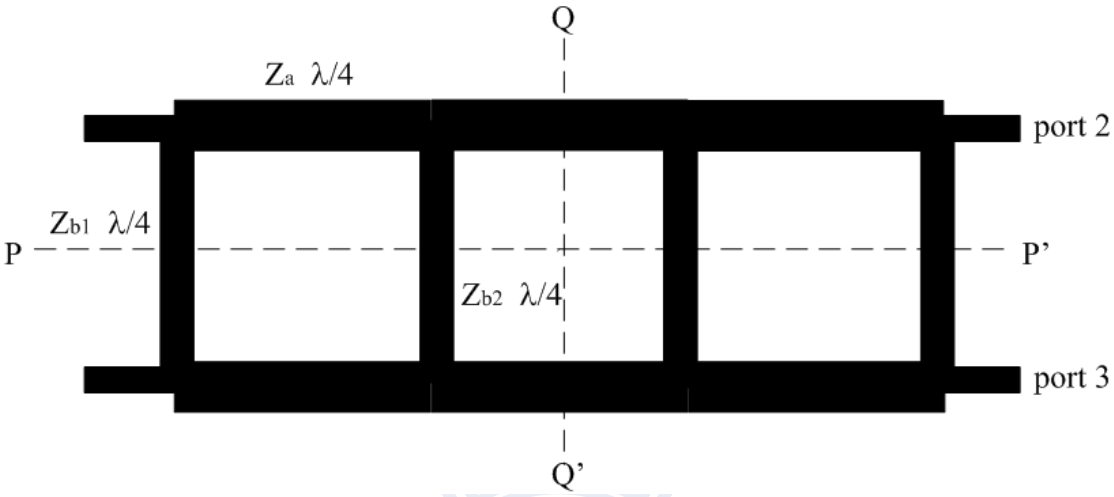

Fig. 2-4. A 3-section branch-line coupler with characteristic impedance Z_a for main line and Z_{b1} and Z_{b2} for branch lines.

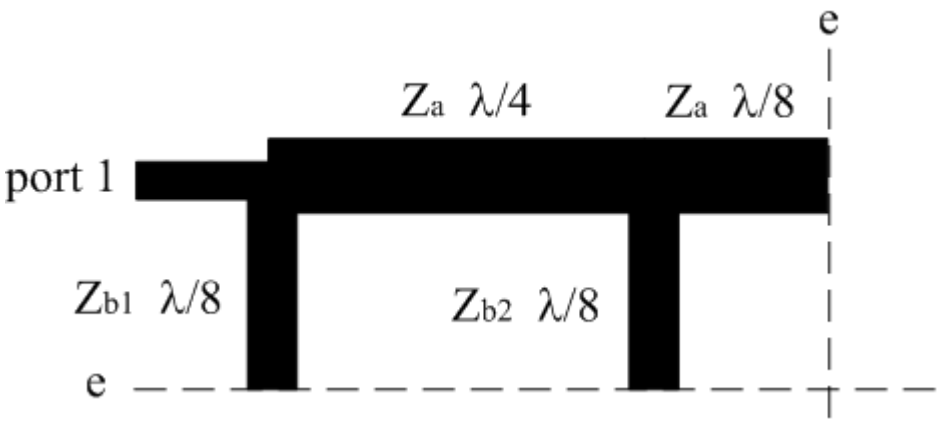

(a)

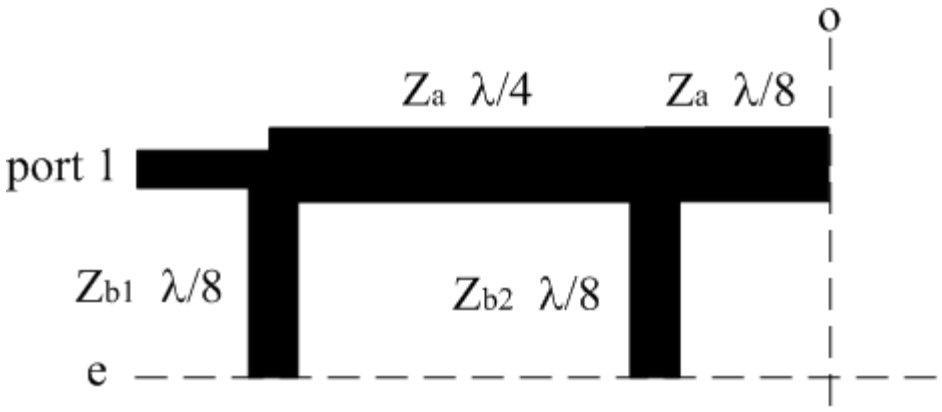

(b)

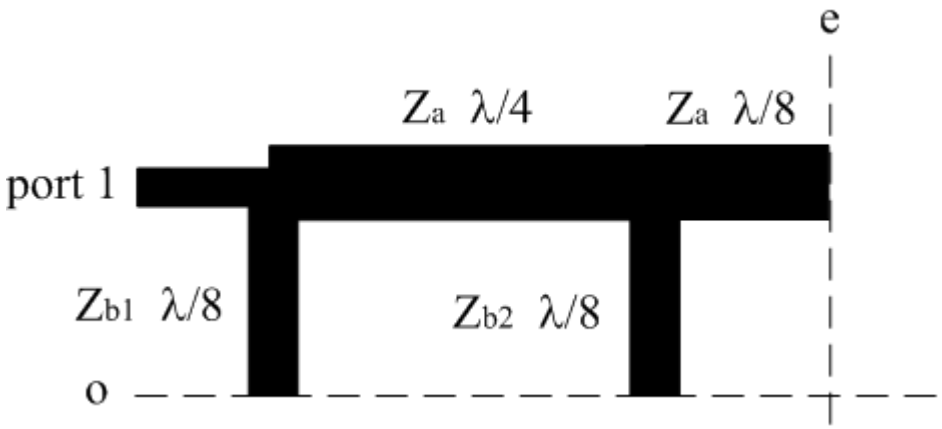

(c)

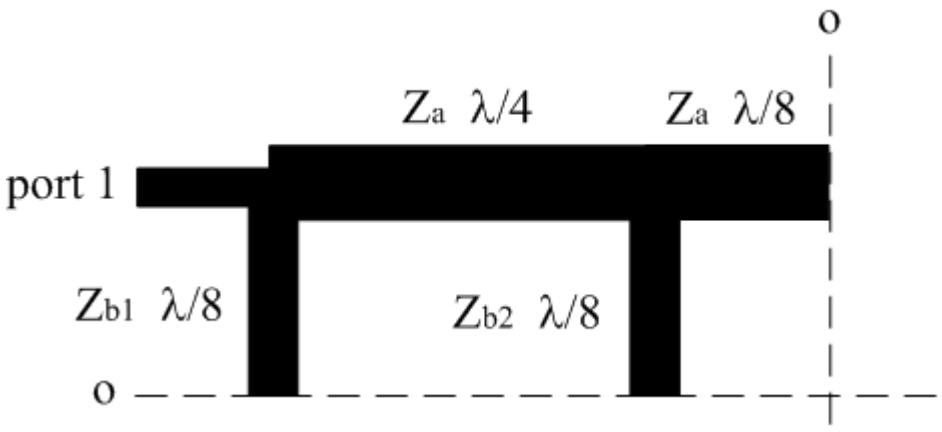

(d)

Fig. 2-5. Even/odd mode analysis for the bisymmetric circuit in Fig. 2-4. (a) Even-even mode (b) Even-odd mode (c) Odd-even mode (d) Odd-odd mode

Fig. 2-4 shows layout of a 3-section branch-line coupler. In analysis, the *PP'* and *QQ'* planes can be assigned as either an electric or a magnetic wall. Fig. 2-5 (a) through (d) shows the reduced equivalent circuit of 3-section branch-line coupler when PP' and QQ' planes are assigned as electric or magnetic walls, the resultant circuit may have four configurations: even-even, even-odd, odd-even, and odd-odd. Note that y_a, y_{b1} and y_{b2} stands for $\frac{Z_a}{Z_0}, \frac{Z_{b1}}{Z_0}$ and $\frac{Z_{b2}}{Z_0}$ respectively. Then, the four input impedances can be derived as follows:

$$y_{ee} = jy_{b1} - \frac{jy_a^{\,2}}{y_{b2} + y_a} \tag{2.8a}$$

$$y_{eo} = jy_{b1} - \frac{jy_a^{\,2}}{y_{b2} - y_a} \tag{2.8b}$$

$$y_{oe} = -jy_{b1} + \frac{jy_a^{\,2}}{y_{b2} - y_a} \tag{2.8c}$$

$$y_{oo} = -jy_{b1} + \frac{jy_a^{\,2}}{y_{b2} + y_a} \tag{2.8d}$$

The S parameters can be written as:

$$S_{11} = \frac{\Gamma_{ee} + \Gamma_{eo} + \Gamma_{oe} + \Gamma_{oo}}{4} \tag{2.9a}$$

$$S_{21} = \frac{\Gamma_{ee} - \Gamma_{eo} + \Gamma_{oe} - \Gamma_{oo}}{4} \tag{2.9b}$$

$$S_{31} = \frac{\Gamma_{ee} - \Gamma_{eo} - \Gamma_{oe} + \Gamma_{oo}}{4} \tag{2.9c}$$

$$S_{41} = \frac{\Gamma_{ee} + \Gamma_{eo} - \Gamma_{oe} - \Gamma_{oo}}{4} \tag{2.9d}$$

where $\Gamma_{ij} = \dfrac{1 - y_{ij}}{1 + y_{ij}}$, the subscripts i and j stand for either e or o.

Based on the input matching and isolation conditions, $S_{11} = S_{41} = 0$, we have:

$$\Gamma_{ee} = -\Gamma_{eo} \tag{2.10a}$$

$$\Gamma_{oe} = -\Gamma_{oo} \tag{2.10b}$$

For simplicity, the imaginary number j is extracted from y_{ij}, i.e. $y_{ee} = ja$, $y_{ee} = jb$, $y_{ee} = jc$ and $y_{ee} = jd$. Equating the real part and imaginary part in (2.10a) and (2.10b), we obtain $1 - a^2 b^2 = 0$ and $(a + b)(ab + 1) = 0$. In addition, c and d have the same relation as a and b. The conditions in (2.9) can be replaced with the following conditions for input admittances:

$$ab = -1 \tag{2.11a}$$

$$cd = -1 \tag{2.11b}$$

In order to specify arbitrary power division $\alpha^2 : 1$, $\dfrac{S_{21}}{S_{31}} = j\alpha$ builds up the relationship between a and c as:

$$\frac{ac + 1}{c - a} = -\alpha \tag{2.12}$$

Substituting *a*, *b*, *c* and *d* into (2.11a) and (2.11b), one can observe that both equations give the same result:

$$1+{y_{b1}}^2+{y_a}^2\frac{{y_a}^2-2y_{b1}y_{b2}}{{y_{b2}}^2-{y_a}^2}=0 \tag{2.13}$$

Using (2.12), (2.13) can be reduced into a result that ${y_a}^2$ is in terms of y_{b1} and y_{b2}:

$${y_a}^2=\frac{{y_{b2}}^2(1-\alpha y_{b1})}{1-\alpha(y_{b1}+y_{b2})} \tag{2.14}$$

Substituting (2.14) into (2.13), y_2 can be expressed in terms of y_{b1}:

$$y_{b2}=\frac{\left(\alpha\left({y_{b1}}^2-1\right)-2y_{b1}\right)(\alpha y_{b1}-1)}{1+\alpha^2} \tag{2.15}$$

Note that y_{b1} is one degree of freedom to be determined for desired fractional bandwidth demonstrated in the following discussion.

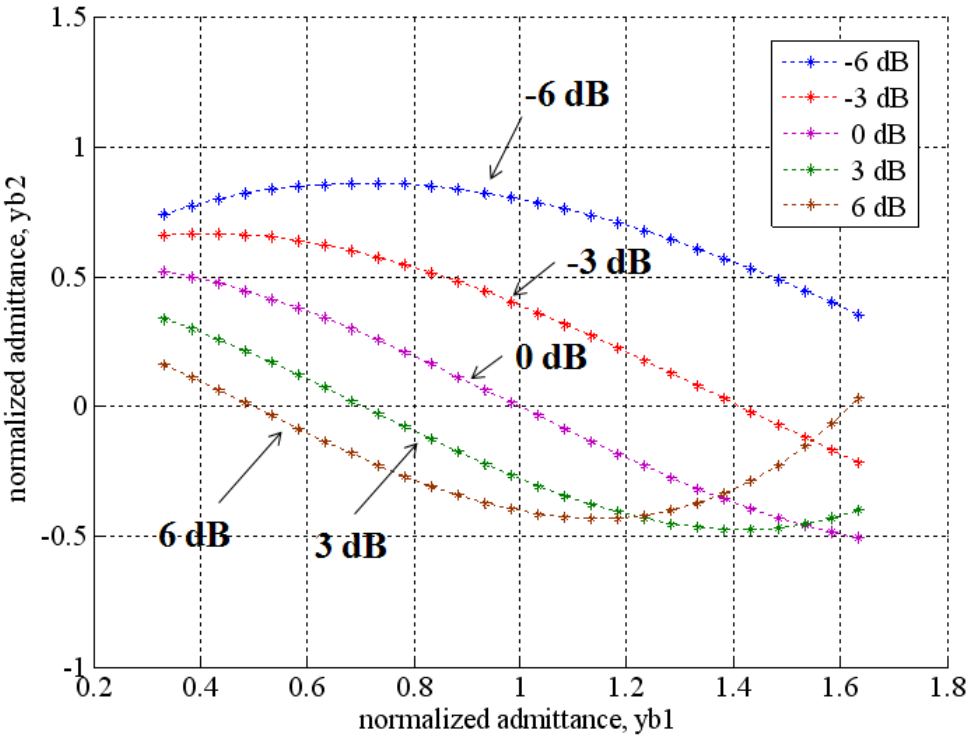

Fig. 2-6. Normalized characteristic admittance y_{b2} with various y_{b1}.

Fig. 2-6 plots the solutions for y_{b2} with various y_{b1} for design of α = -6dB ~ 6dB 3-section branch-line coupler. For fabrication consideration, y_{b1} is assumed from 0.333 to 1.667, i.e., 150 ohm and 30 ohm for $Z_0 = 50\Omega$. It shows that the feasible region of y_{b2} decreases as the power division is increased because y_{b2} must be a positive number larger than 0.333. For instance, for α = 6dB power division design, y_{b2} is only 0.163, or $Z_{b2} = 306.7$ ohm, while $y_{b1} = 0.333$. It also implies that if the more power transmitted to the through port, the higher impedance the branch line has.

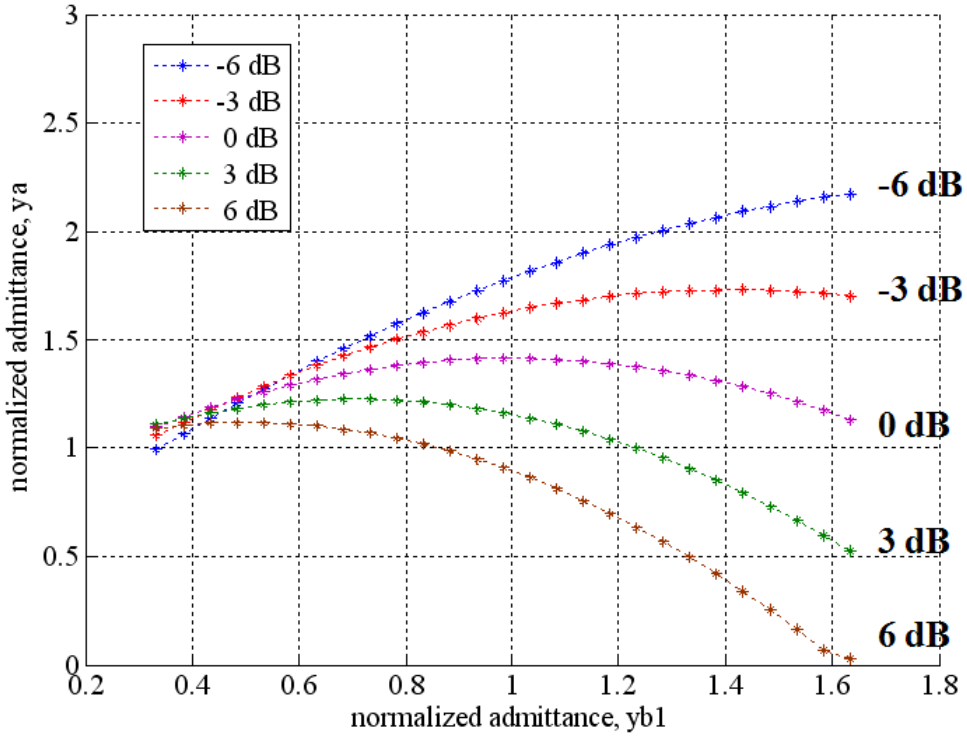

Fig. 2-7. Normalized characteristic admittance y_a with various y_{b1}.

Fig. 2-7 shows the solutions changes of y_a with respec to various y_{b1} to design of -6dB ~ 6dB power division. Obviously, one can see that the variation of y_a is more moderate than y_{b2} and y_a is always positive while $0.333 < y_{b1} < 1.667$. Besides, for 6dB and -6dB design, the slope of y_a with respect to y_{b1} is positive for -6dB and negative for 6dB. This result is similar to that of y_{b2}.

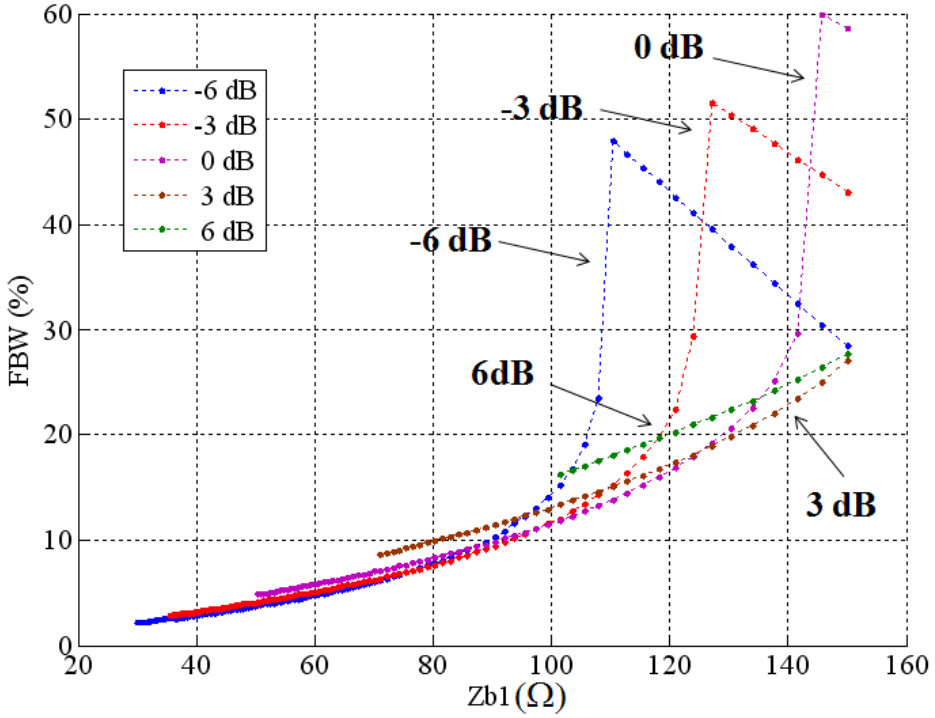

(a)

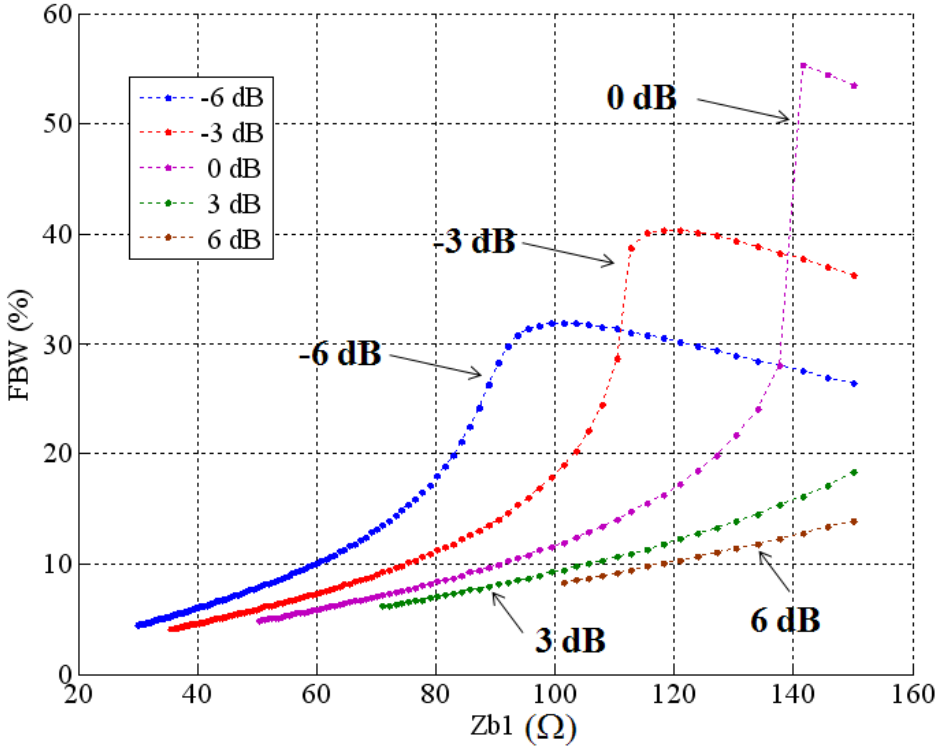

(b)

Fig. 2-8. The variation of -20dB fractional bandwidth with various Z_{b1}. (a) S_{11} (b) S_{41}

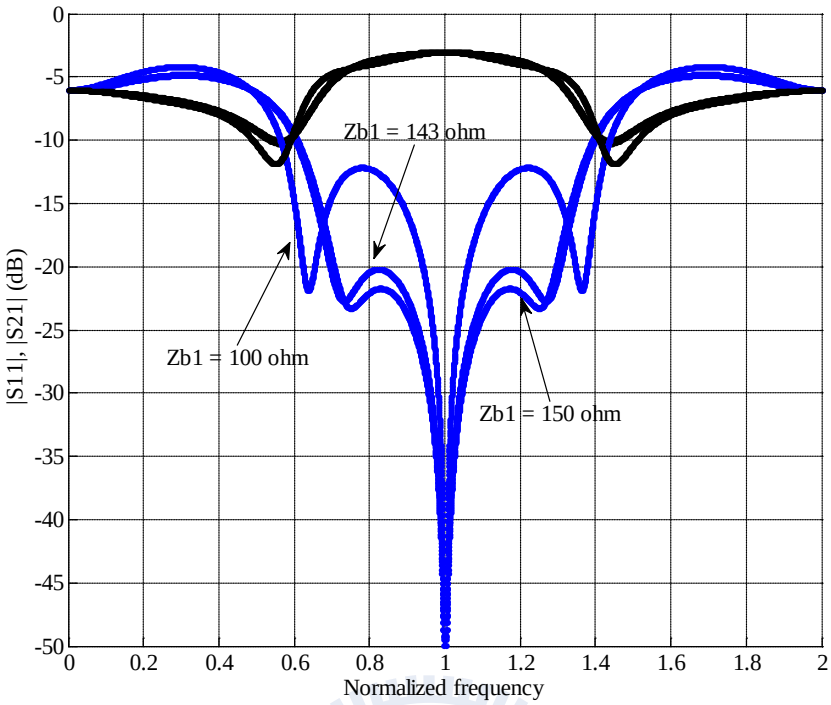

(a)

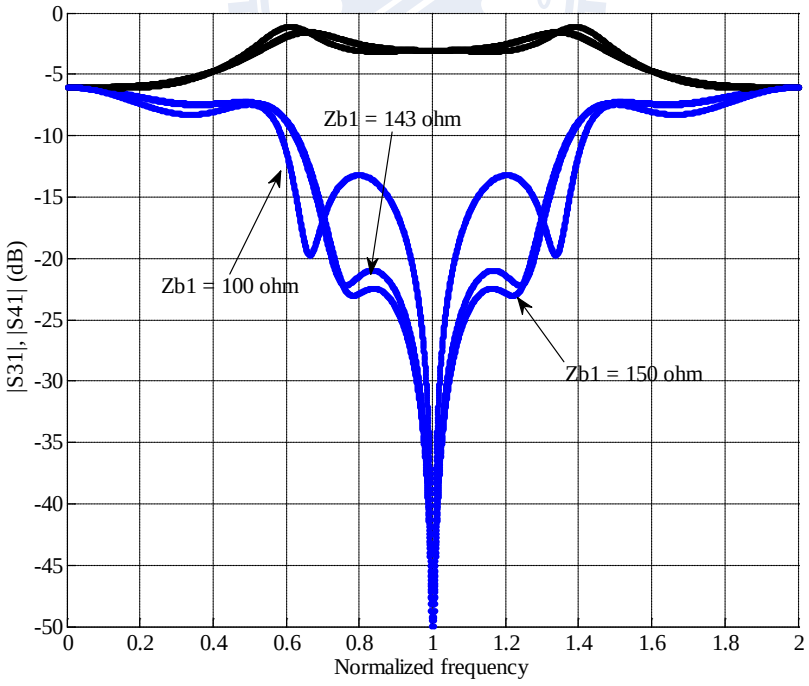

(b)

Fig. 2-9 Illustrations for the discontinuity points of the fractional bandwidth prediction. (a) $|S_{11}|$ and $|S_{21}|$ (b) $|S_{31}|$ and $|S_{41}|$

Fig. 2-8 (a) and (b) plot the fractional bandwidth of a 3-section branch-line coupler with various Z_{b1} for power division of -6 dB to 6 dB. The fractional bandwidths are defined as the frequency band in which the magnitude of the *S*-parameter is -20dB. One can see that the bandwidth increases while Z_{b1} is increased. Note that there is one discontinuity point, for instance, the maximum fractional bandwidth of S_{11} for 0dB design occurs when Z_{b1} is approximately 143 ohm. Investigating the frequency response shown in Fig. 2-9, the bandwidth is located in a narrow window when Z_{b1} is smaller than 143 ohm, and the bandwidth suddenly becomes maximum because the two local maxima are lower than -20 dB defined as the fractional bandwidth. Interestingly, the bandwidth again decreases when Z_{b1} is larger than that point. After simulating some solutions near the corner, one can see that the two local maximums vanish gradually and simultaneously the bandwidth becomes narrower. The desired wideband branch-line coupler with specific fractional bandwidth can be designed according to this graph. Table 2-1 compares the maximal fractional bandwidths with various power divisions.

Table 2-1
Summary Data of the Maximal Fractional Bandwidth for $|S_{11}|$ and $|S_{41}|$

Power division	*FBW of $\|S_{11}\|$ (Z_{b1})	*FBW of $\|S_{41}\|$ (Z_{b1})
-6 dB	48.56% (109.1 Ω)	31.89% (101.4 Ω)
-3 dB	52.22% (125.5 Ω)	40.33% (118.1 Ω)
0 dB	60.67% (143.5 Ω)	55.78% (139.5 Ω)
3 dB	27.11% (150.0 Ω)	18.33% (150.0 Ω)
6 dB	27.78% (150.0 Ω)	14.0% (150.0 Ω)

* the FBWs of $|S_{11}|$ and $|S_{41}|$ are in reference of -20 dB.

2.2.2 Simulation

Herein, only simulations are demonstrated to verify the idea because the miniaturized circuits are focused in this thesis and will be presented in next chapter. Two circuits are simulated to confirm the formulation by the software package IE3D [22]. The substrate has dielectric constant ε_r = 2.2 and thickness h = 0.508 mm. One circuit demonstrated is specified for -3 dB power division and the other for 3 dB power division, both with maximal fractional bandwidth of $|S_{41}|$. The operating frequency is 1 GHz.

Fig. 2-10 shows the 3-section branch-line coupler with -3 dB power division. In Fig. 2-8 (b), the impedances of Z_{b1}, Z_{b2}, and Z_a are 125.12 Ω, 75.0169 Ω, and 43.9481 Ω, respectively. The circuit size is 163.5 mm×59.03 mm. Fig. 2-11 (a) plots the magnitude responses of the *S*-parameters when the signal is excited at port 1, the simulation data at f_o show that $|S_{11}|$ = –49.18 dB, $|S_{21}|$ = –5.19 dB, $|S_{31}|$ = -2.24 dB and $|S_{41}|$ = –49.18 dB. The bandwidths in reference of $|S_{11}|$ < -20 dB and $|S_{41}|$ < -20 dB are 53.7% and 40%, respectively. The relative phase difference between S_{21} and S_{31} is 89.73^0 in Fig. 2-11 (b).

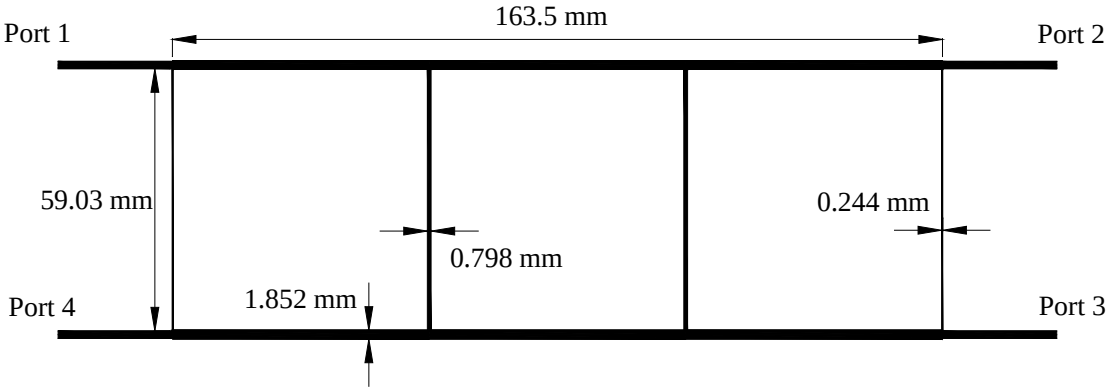

Fig. 2-10. Physical layout for 3-section branch-line coupler with -3dB power division and maximum fractional bandwidth

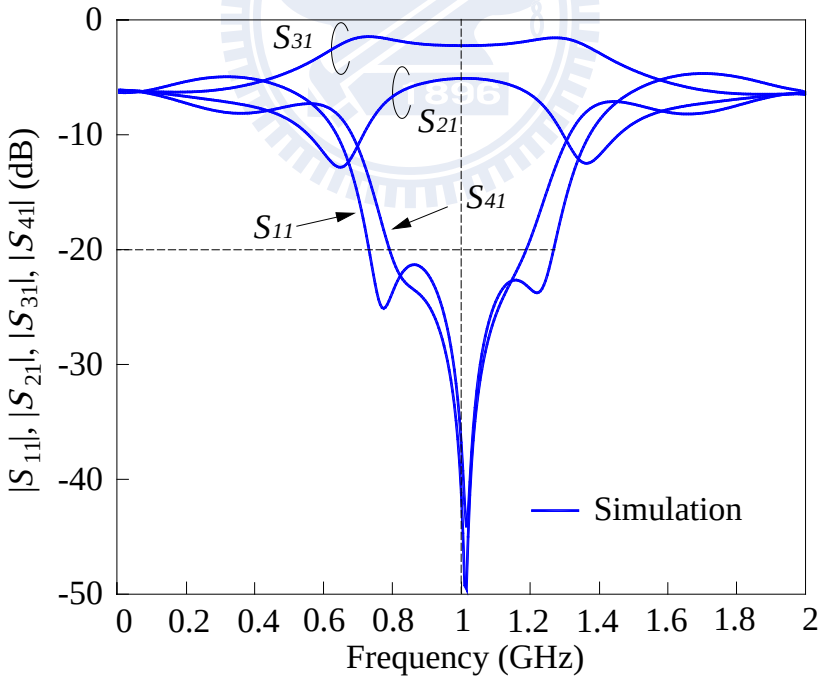

(a)

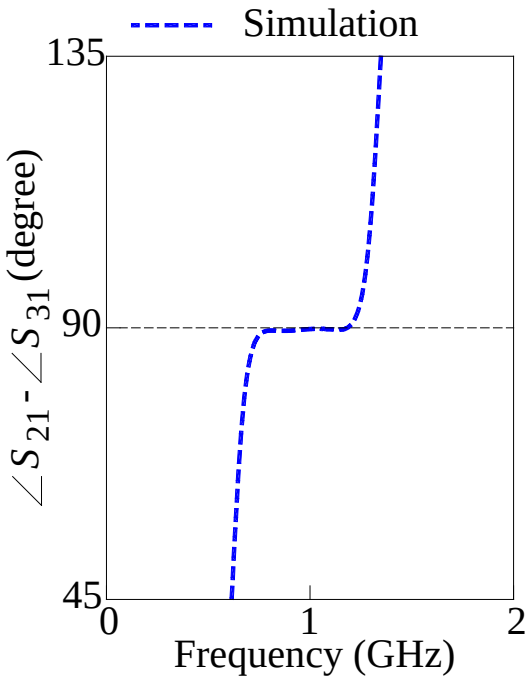

(b)

Fig. 2-11. Simulation for 3-section branch-line coupler with -3dB power division and maximal fractional bandwidth (a) Magnitude response (b) Relative phase response

Fig. 2-12 shows the 3-section branch-line coupler with 3 dB power division. In Fig. 2-8 (b), the impedances of Z_{b1}, Z_{b2}, and Z_a are 150 Ω, 147 Ω, and 45.02 Ω, respectively. The circuit size is 163.47 mm×59.37 mm. Fig. 2-13 (a) plots the magnitude responses of the *S*-parameters when the signal is excited into port 1, the simulation data at f_o show that $|S_{11}|$ = –41.69 dB, $|S_{21}|$ = –2.09 dB, $|S_{31}|$ = -5.22 dB and $|S_{41}|$ = –39.86 dB. The bandwidths in reference of $|S_{11}|$ < -20 dB and $|S_{41}|$ < -20 dB are 28.6% and 19.7%, respectively. The relative phase difference between S_{21} and S_{31} is 89.49^0 in Fig. 2-13 (b). One can observe that the simulation results agree very well with the prediction.

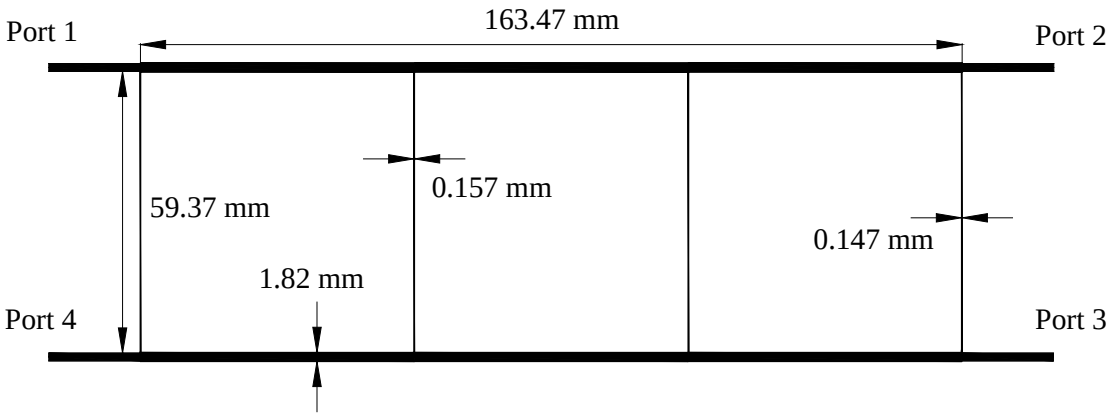

Fig. 2-12. The physical layout for 3-section branch-line coupler with 3 dB power division and maximum fractional bandwidth

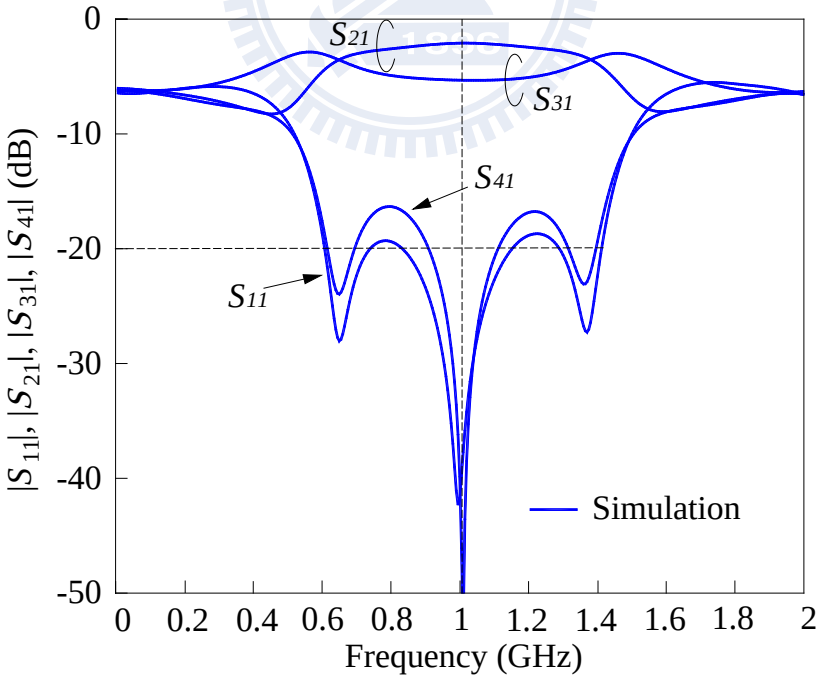

(a)

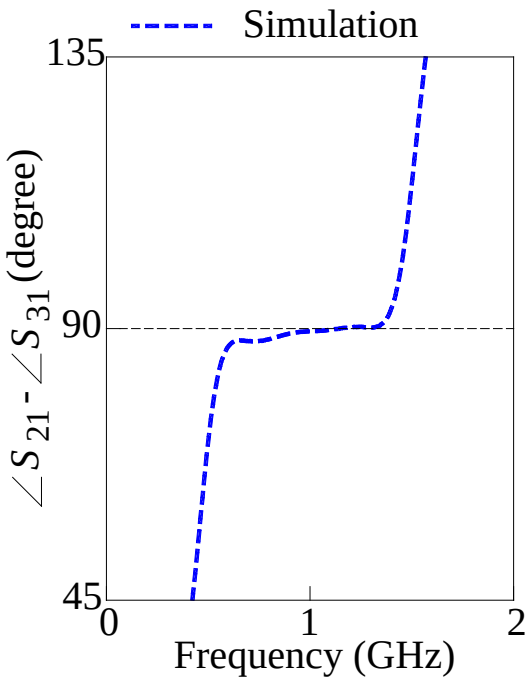

(b)

Fig. 2-13. Simulation for 3-section branch-line coupler with 3 dB power division and maximum fractional bandwidth (a) magnitude (b) phase difference

Based on the principle of branch-line coupler, an extension to have a wide-band branch-line coupler with arbitrary power division and specified fractional bandwidth is performed. Formulation for analyzing the circuit is derived and solution curves are provided. Two circuits are designed and simulated to validate the idea. Good simulation results agree with the design equations and prediction on fractional bandwidth.

Yet, for applications with low operating frequencies, the circuit size implemented by transmission lines is a vital problem due to the miniaturized design trend in modern RF system. Thus, in the next chapter, the miniaturization for a 3-section branch-line coupler is under study.

Chapter 3

Miniaturized 3-Section Branch-Line Coupler by Lumped Distributed - and Lumped Elements

Conventional directional couplers are realized with the use of transmission lines of different types. In MIC, microstrip lines are the most popular transmission line. At frequencies below 20 GHz distributed components occupy large areas and create dimensional problems in MMIC's. Lumped elements are very attractive in applications where size reduction is important. It is known that, at a single frequency, the symmetrical π- or T- LC section is equivalent to the transmission line section with the appropriate characteristic impedance and electrical length. Consequently, the lines which compose a coupler can be partially or completely replaced by lumped sections.

In this chapter, miniaturized 3-section branch-line coupler is implemented by replacing the transmission lines with equivalent circuit models which composes lumped elements such as capacitors and inductors. First, analysis on equivalent circuit models is presented. Then, using these equivalent circuit models, size reduction can be achieved for a 3-section branch-line coupler with good performance.

3.1 Analysis with Equivalent Circuit Models.

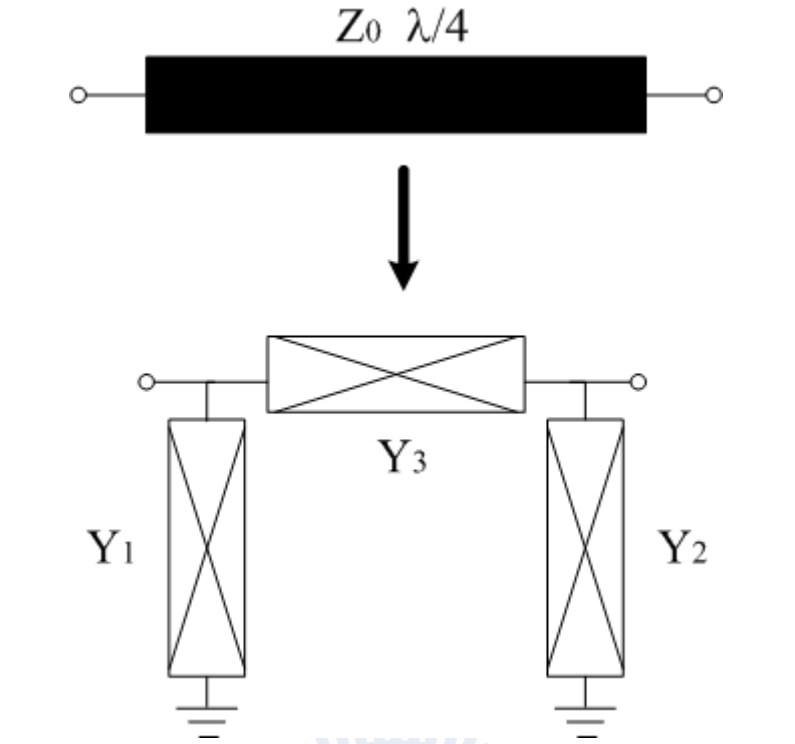

(a)

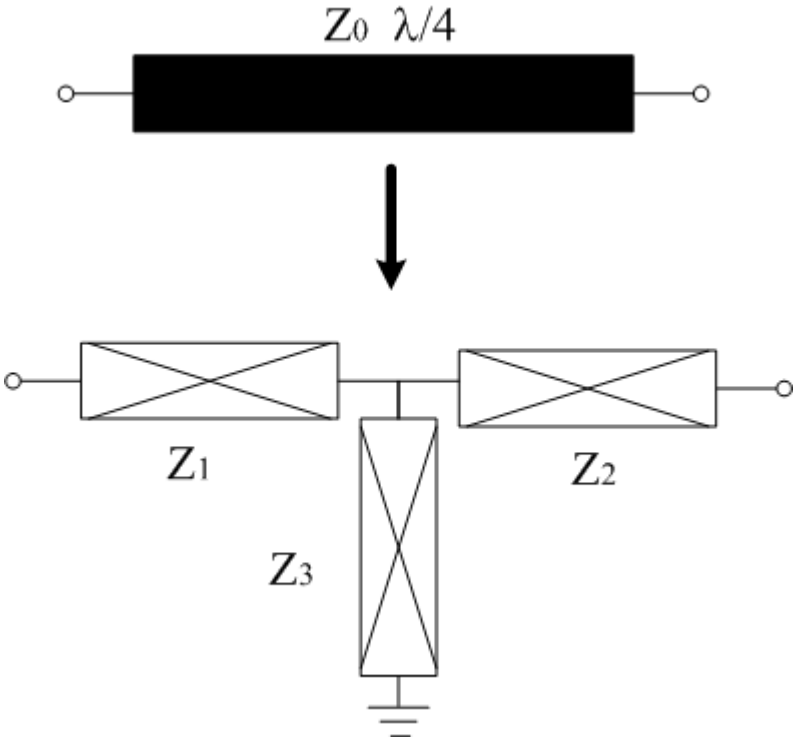

(b)

Fig. 3-1. Equivalent circuit models for one section of transmission line with arbitrary electrical length θ and characteristic impedance Z_0. (a) π model. (b) T model.

Fig. 3-1 shows two equivalent circuit models for a section of transmission line with arbitrary electrical length θ and characteristic impedance Z_0. For equivalence, the ABCD matrices of a transmission line and π network should be identical:

$$ABCD_{TL} = \begin{bmatrix} \cos\theta & jZ_0 \sin\theta \\ jY_0 \sin\theta & \cos\theta \end{bmatrix}$$

$$ABCD_{lumped,\pi} = \begin{bmatrix} 1 & 0 \\ Y_1 & 1 \end{bmatrix} \begin{bmatrix} 1 & \frac{1}{Y_2} \\ 0 & 1 \end{bmatrix} \begin{bmatrix} 1 & 0 \\ Y_3 & 1 \end{bmatrix}$$

$$= \begin{bmatrix} 1+\frac{Y_2}{Y_3} & \frac{1}{Y_3} \\ Y_1 + Y_2 + \frac{Y_1 Y_2}{Y_3} & 1+\frac{Y_1}{Y_3} \end{bmatrix}$$

One can see that due to symmetry of a transmission line section, Y_1 and Y_2 must be the same such that the degrees of freedom reduce from 3 to 2. Take the π model as an example, the network has a low-pass function if Y_1 and Y_3 are shunt capacitors with a series inductor Y_2. After some mathematical manipulations, the values of capacitance and the inductance can be derived as follows:

$$\omega L = Z_0 \sin\theta$$

$$\omega C = \frac{1}{Z_0} \tan\frac{\theta}{2}$$

Similarly, the network with the high-pass characteristic has the following capacitance and inductance:

$$\omega L = Z_0 \cot\frac{\theta}{2}$$

$$\omega C = \frac{1}{Z_0 \sin\theta}$$

Note that the capacitance and inductance for the π model with low-pass characteristic are exactly the inverse of the inductance and capacitance for the π model with high-pass characteristic, respectively.

For T models, all capacitances and inductances can be derived with the same approach instead of replacing with the ABCD matrix of T model:

$$ABCD_{lumped,T} = \begin{bmatrix} 1+\frac{Z_1}{Z_3} & Z_1 + Z_2 + \frac{Z_1 Z_2}{Z_3} \\ \frac{1}{Z_3} & 1+\frac{Z_2}{Z_3} \end{bmatrix}$$

Table 3-1 lists the formula for equivalent circuit models with various electrical lengths 30^0, 45^0 and 90^0. For instance, assuming operating frequency is at 1 GHz and Z_0 = 50 Ω, the values of capacitances and inductance are calculated for reference. Note that the sign + stands for equivalent models with low-pass characteristic and the sign − for equivalent models with high-pass characteristic.

Table 3-1

Examples of Equivalent Circuit Models with Various Electrical Lengths

f_0@1 GHz, Z_0 = 50 ohm	formulation		30^0	45^0	90^0
π+ model	$\omega L = Z_0 \sin\theta$	L (nH)	3.979	5.627	7.958
	$\omega C = \frac{1}{Z_0}\tan\frac{\theta}{2}$	C (pF)	0.853	1.318	3.183
π – model	$\omega L = Z_0 \cot\frac{\theta}{2}$	L (nH)	29.699	19.212	7.958
	$\omega C = \frac{1}{Z_0 \sin\theta}$	C (pF)	6.366	4.502	3.183
T+ model	$\omega L = Z_0 \tan\frac{\theta}{2}$	L (nH)	2.132	3.296	7.958
	$\omega C = \frac{\sin\theta}{Z_0}$	C (pF)	1.592	2.251	3.183
T – model	$\omega L = \frac{Z_0}{\sin\theta}$	L (nH)	15.915	11.254	7.958
	$\omega C = \frac{1}{Z_0}\cot\frac{\theta}{2}$	C (pF)	11.879	7.685	3.183

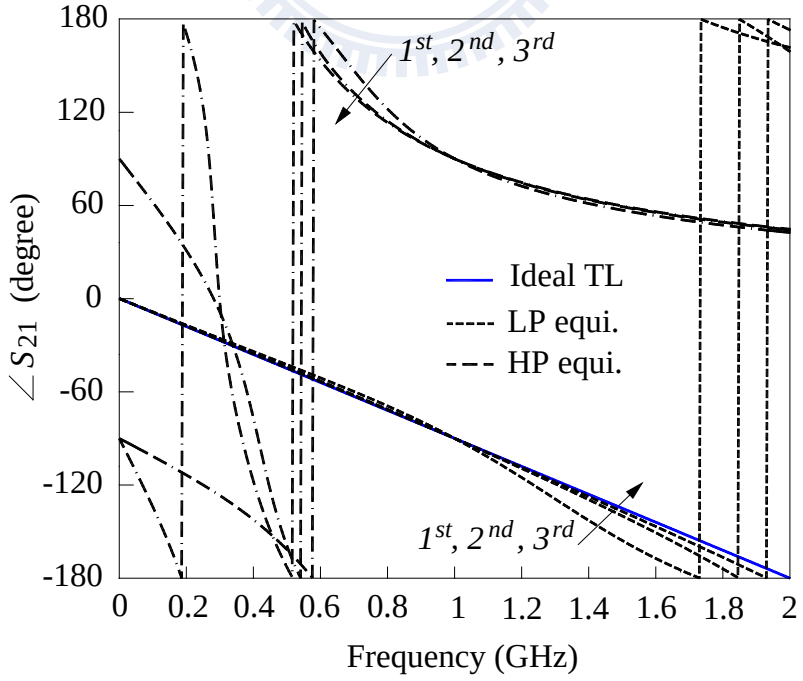

Fig. 3-2. Phase response of S_{21} for equivalent circuit models with θ = 30^0, 45^0, and 90^0.

Fig. 3-2 plots the phases of S_{21} for π models with 1st-, 2nd- and 3rd order models equivalent to one transmission line of 90^0. One can see that higher order equivalence gives a better approximation. Interestingly, 2nd order model improves the performance much better than the 1st-order one, but the 3rd-order model brings comparatively slight improvement on 2nd-order model. For instance, for a conventional branch-line coupler with 0 dB power division, Fig. 3-3 plots the frequency responses with multi-section equivalent circuit models. The circuit implemented by transmission lines has the FBW 10.5% and the others with 8.12%, 9.45% and 9.95% for 1st-order one to 3rd order, respectively. One can conclude that the 2nd order equivalence is slightly not good as the 3rd-order one, but for lower frequency application, 2nd order model is adequate to approximate a transmission line. Later, the 2nd order model is adopted in consideration of fabrication complexity. Note that the same characteristics described for π models appear in the T models.

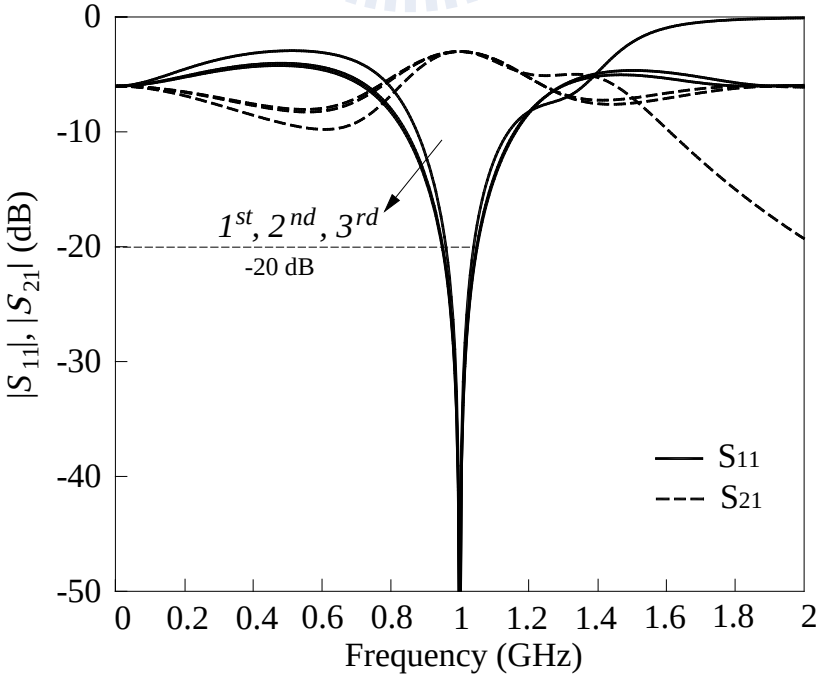

(a)

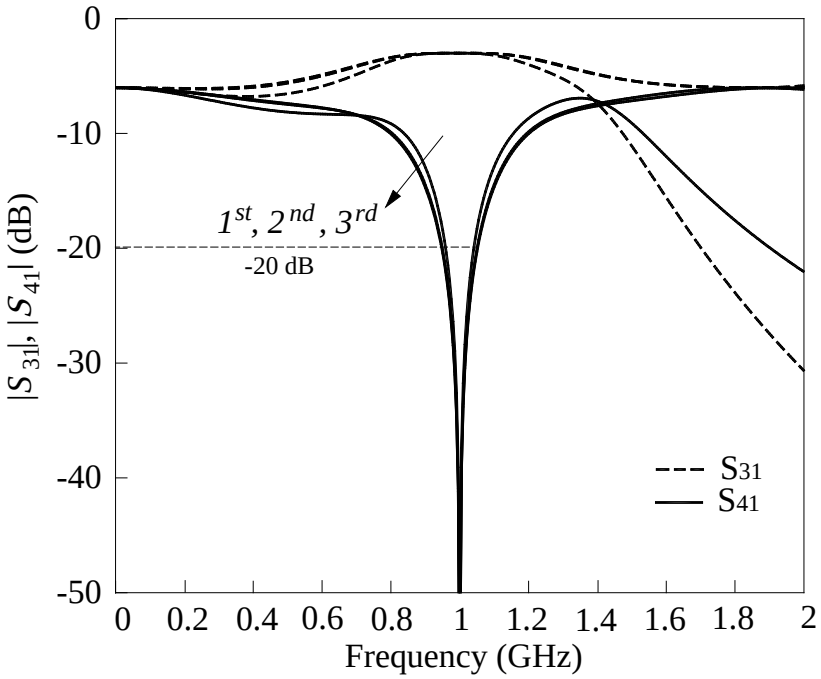

(b)

Fig. 3-3. Variations of frequency responses with 1st order, 2nd order and 3rd order equivalence. (a) $|S_{11}|$ and $|S_{21}|$ (b) $|S_{31}|$ and $|S_{41}|$

3.2 Miniaturization by Lumped Distributed Elements

One 3-section branch-line coupler designed at 1 GHz with -3 dB power division and optimal fractional bandwidth is fabricated and measured for demonstration. Fig. 3-4 (a) and (b) shows the layout. The substrate has a relative dielectric constant ε_r = 2.2 and thickness h = 0.508 mm. The 2-section T network equivalent circuit models for a transmission line section of electrical length $+90^0$ and characteristic impedances of 125.12 Ω, 75.0169 Ω , and 43.9481 Ω are used. The circuit is simulated and optimized by the software package ADS [23].

Table 3-2 lists the values used in theory and optimization. The surface mount devices (SMDs) of 0805 are employed. For SMDs, there are some typical values for capacitors and inductors, thus optimization is subject to available values. Note that the

shunt capacitors of outer-side branch lines are replaced by open stubs of 50 ohm with appropriate electrical lengths. Using the shunt open stubs brings two advantages: one is controllable variance of transmission line during fabrication with low complexity; the other is design flexibility due to limited lumped element values. In view of physics, a wider line width corresponds to a larger capacitance. Yet, the coupling effect between the open stubs occurs when the lines are tightly close coupled. Typically, there is a three-time distance reserved between two transmission lines in case of coupling.

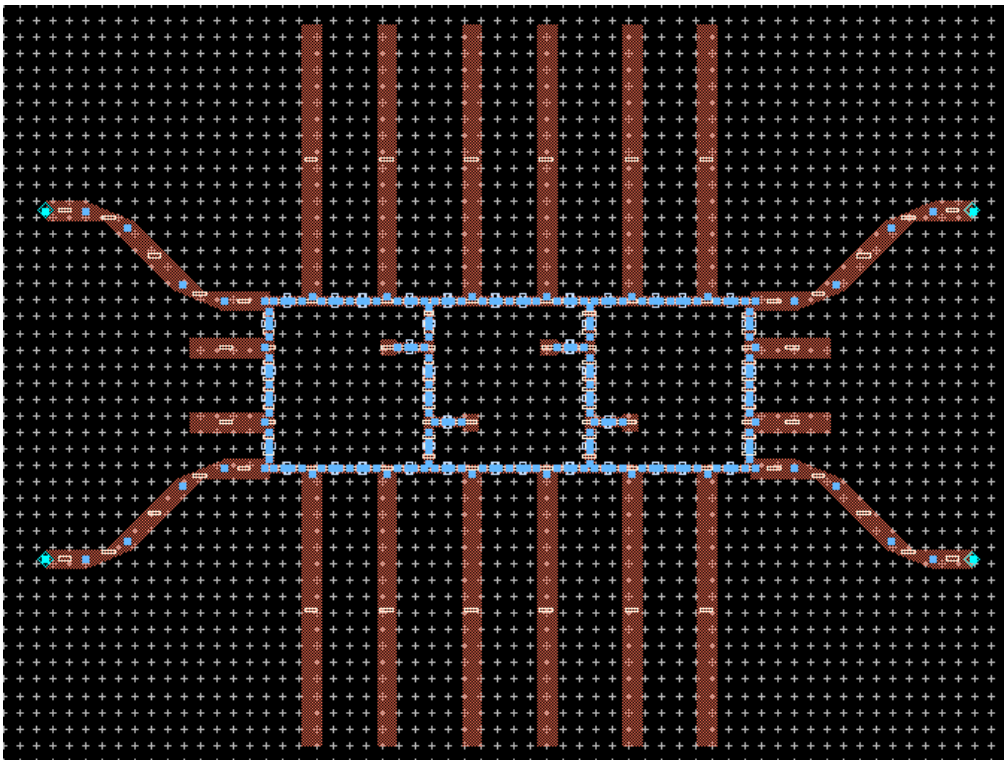

(a)

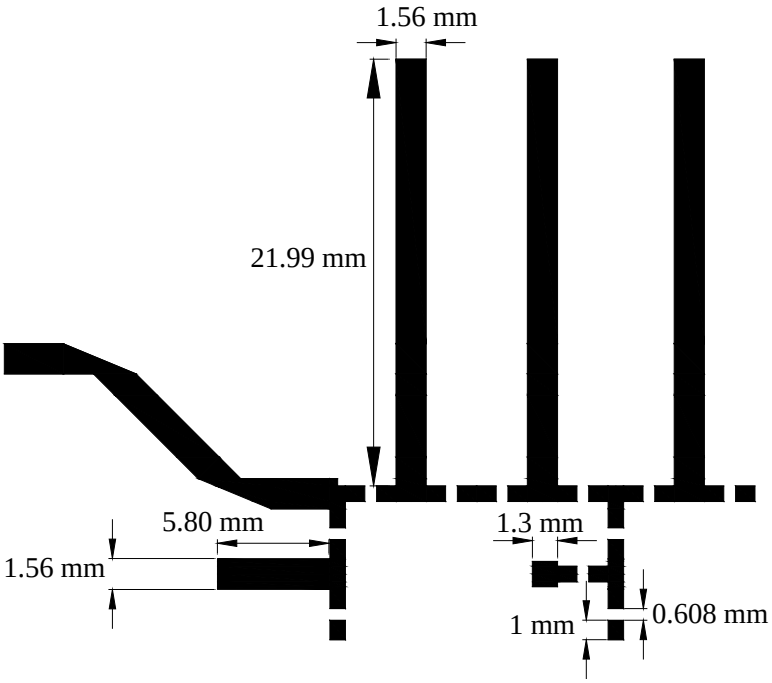

(b)

Fig. 3-4. (a) Layout of 3-section branch-line coupler with -3 dB power division in ADS (Circuit 1) (b) geometric parameters of the quarter circuit.

.

Table 3-2

Summary Data of the Lumped/Distributed Element Values

	Theory		Optimal
L_{b1} (nH)	8.3802	L_{b1} (nH)	10
L_{b2} (nH)	4.9471	L_{b2} (nH)	4.7
L_a (nH)	2.9162	L_a (nH)	3.3
C_{b1} (pF)	0.8853	Open stub	50ohm, 5.8^0
C_{b2} (pF)	1.4997	C_{b2} (pF)	1.0
C_a (pF)	2.5441	Open stub	50ohm, 21^0

Two of the four ports of the coupler circuit are connected to a HP8720ES network analyzer using coaxial cables and the other two ports are terminated in 50 ohm resistances, to measure the circuit. The conventional short-open-load-through (SOLT) calibration method is applied to eliminate the effects of the cables. Fig. 3-5 shows the simulated and measured results. Fig. 3-5 (a) and (b) plot $|S_{11}|$, $|S_{21}|$, $|S_{31}|$, and $|S_{41}|$ responses. Obviously, there is discrepancy that the designed band drifts toward lower frequency caused by the practical inductances of the surface mount inductors with certain variation. At the operating frequency, $|S_{11}|$ and $|S_{41}|$ are below -25 dB, while $|S_{21}|$ and $|S_{31}|$ are -6.86 dB and -2.36 dB; both one lower than the theoretical results. This can be ascribed to the non-ideal lumped elements with parasitic resistances. The measurement indicates that the circuit has bandwidths of 33.15% and 28.28% for $|S_{11}|$ and $|S_{41}|$, respectively, for a reference of -20 dB. Fig. 3-5 (c) shows the response of relative phase $\angle S_{31}$-$\angle S_{21}$ which is 96.54^0 at 1 GHz. This degradation of the phase difference is due to parasitic inductance and capacitance of chip devices. Fig. 3-6 shows the photograph of the experimental circuit. Table 3-3 shows the summary data of simulation and experiment.

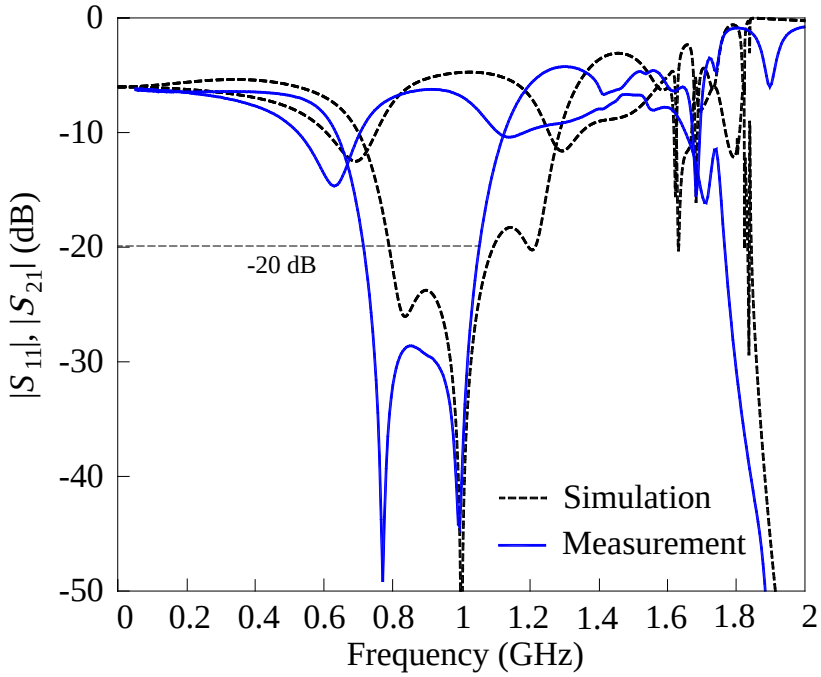
0
-10
-20
-30
-40
-50
-20 dB
Simulation
Measurement
0 0.2 0.4 0.6 0.8 1 1.2 1.4 1.6 1.8 2
Frequency (GHz)
|S11|, |S21| (dB)

(a)

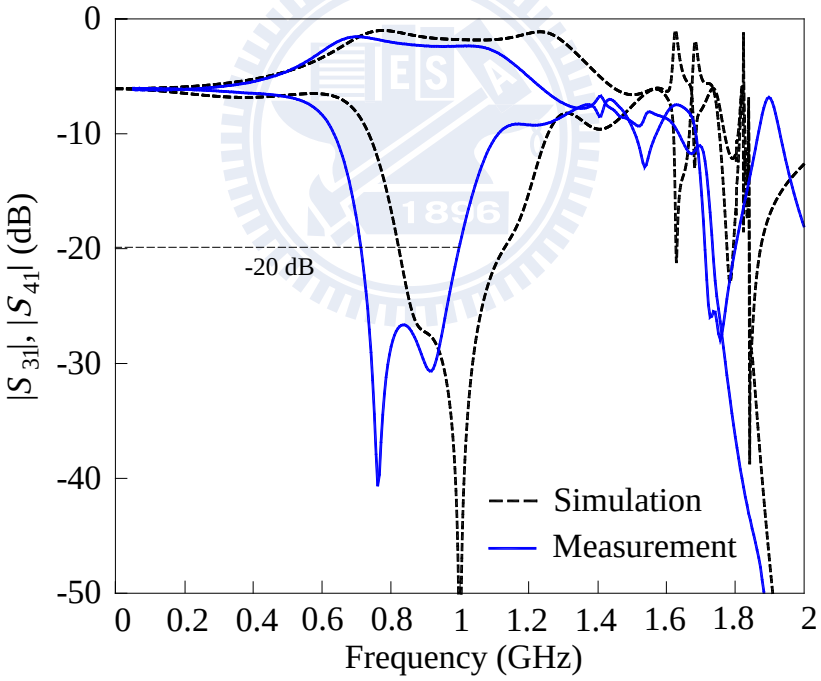
0
-10
-20
-30
-40
-50
-20 dB
Simulation
Measurement
0 0.2 0.4 0.6 0.8 1 1.2 1.4 1.6 1.8 2
Frequency (GHz)
|S31|, |S41| (dB)

(b)

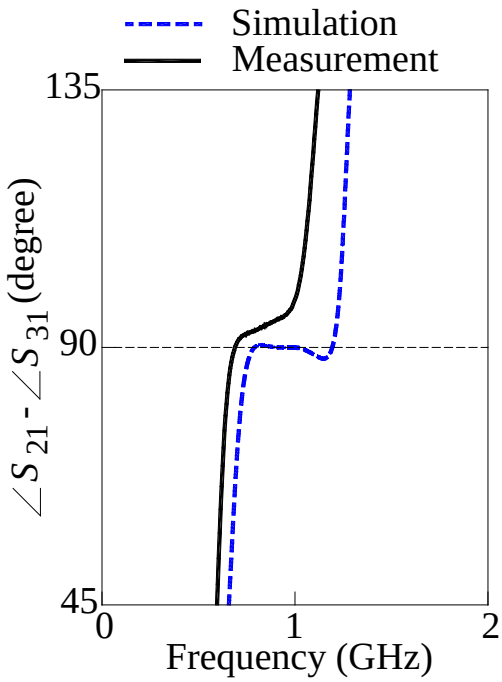

(c)

Fig. 3-5 Simulation and measurement of the 3-section branch-line coupler. (a) $|S_{11}|$ and $|S_{21}|$ (b) $|S_{31}|$ and $|S_{41}|$. (c) The simulation and measurement of phase difference between S_{21} and S_{31}.

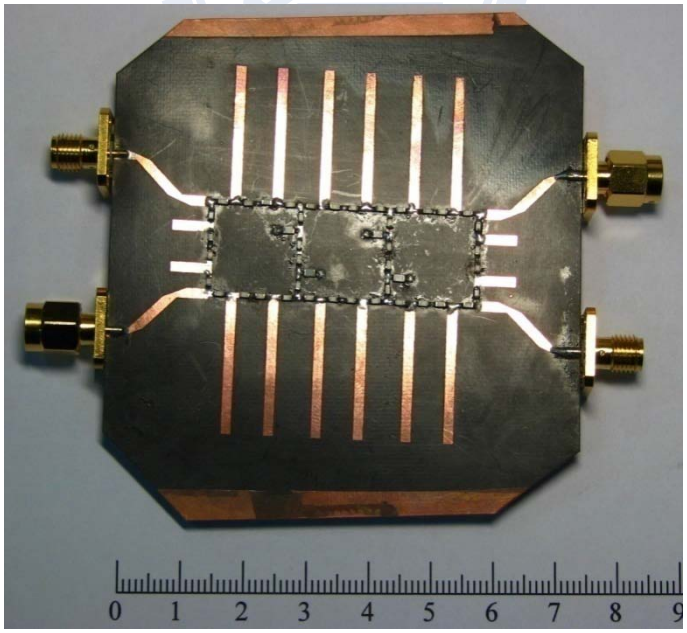

Fig. 3-6. The photo of the Circuit 1

Table 3-3

Summary Data of the 3-Section Branch-Line Coupler with -3dB Power Division

(Circuit 1)

	Simulation	Measurement
Operating frequency	1 GHz	1 GHz
Return Loss ($\|S_{11}\|$)	-66.41 dB	-40.60 dB
FBW*	30.3%	33.15%
Through ($\|S_{21}\|$)	-4.76 dB	-6.86 dB
Coupling ($\|S_{31}\|$)	-1.77 dB	-2.36 dB
Isolation ($\|S_{41}\|$)	-68.17 dB	-19.56 dB
FBW	30.4%	28.28%
$\angle S_{21} - \angle S_{31}$	89.99^0	96.54^0

* FBWs are in reference of -20 dB level.

3.3 Miniaturization by Lumped Elements

In this section, open stubs are replaced with chip capacitors to implement a 3-section branch-line coupler designed at 1 GHz with -3 dB power division and optimal fractional bandwidth. Fig. 3-7 shows the layout. Table 3-4 lists the values used in theory and optimization. The circuit is simulated and optimized by the software package ADS [23].

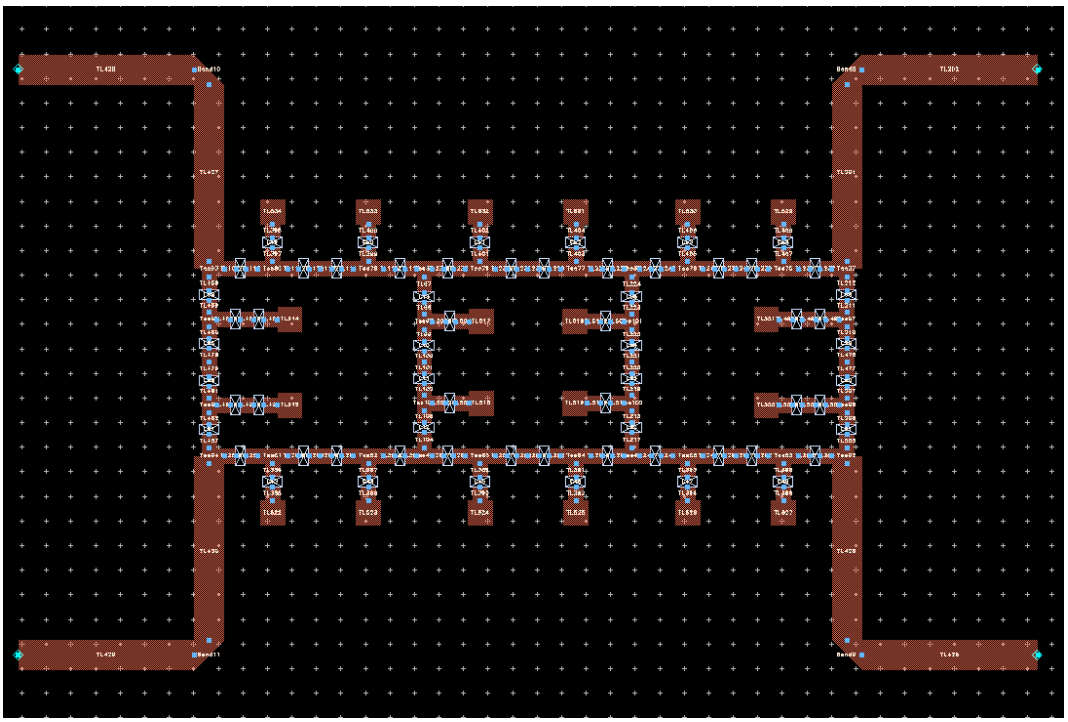

(a)

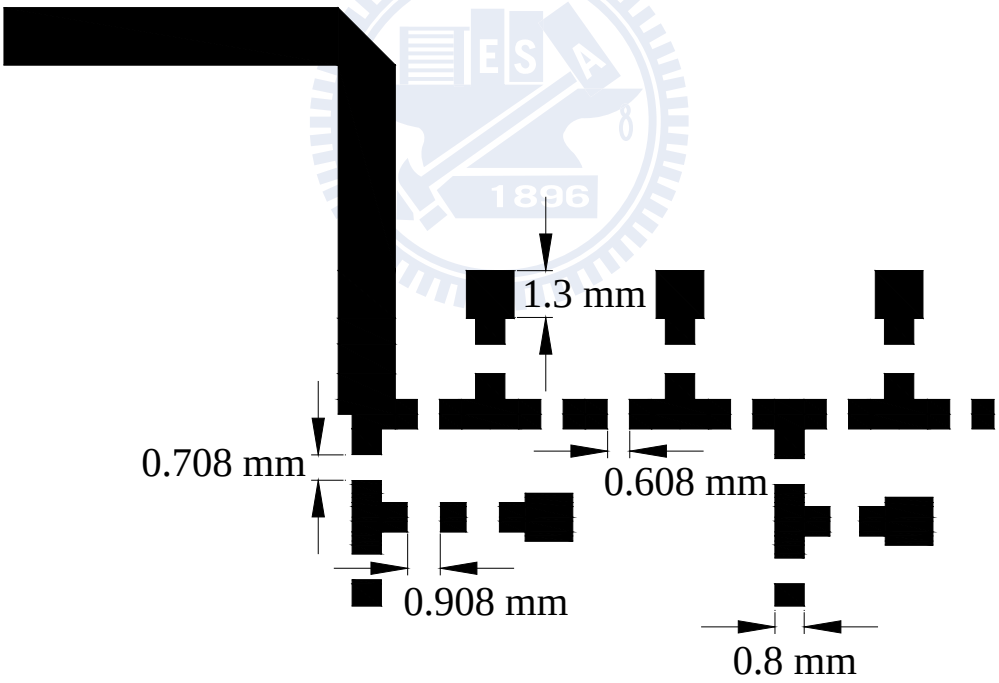

(b)

Fig. 3-7. (a) Layout of 3-section branch-line coupler with -3 dB power division in ADS (Circuit 2). (b) Geometric parameters of the quarter circuit.

.

Table 3-4
Summary Data of the Lumped Element Values

	Theory	Optimal
L_{b1} (nH)	8.3802	10
L_{b2} (nH)	4.9471	4.7
L_a (nH)	2.9162	3.3
C_{b1} (pF)	0.8853	0.5
C_{b2} (pF)	1.4997	1
C_a (pF)	2.5441	2

Fig. 3-8 (a) and (b) plot $|S_{11}|$, $|S_{21}|$, $|S_{31}|$, and $|S_{41}|$ responses. At the operating frequency, $|S_{11}|$ and $|S_{41}|$ are below -20 dB, while $|S_{21}|$ and $|S_{31}|$ are -7.11 dB and -4.66 dB. The measured $|S_{21}|$ and $|S_{31}|$ are lower than the theoretical data because the capacitors and inductors have parasitic resistances that cause severe power dissipation. The measurement indicates that the circuit has bandwidths of 35.59% and 26.33% for $|S_{11}|$ and $|S_{41}|$, respectively, for a reference of –20 dB level. Fig. 3-8 (c) shows the response of relative phase $\angle S_{31}$-$\angle S_{21}$ which is 90.57^0 at 1 GHz. Due to the parasitic inductance and capacitance of SMDs, the fractional bandwidth is narrower than the simulated results with degradation of the phase difference between S_{21} and S_{31}. Fig. 3-9 shows the photograph of the experimental circuit. Table 3-5 shows the summary data of simulation and experiment.

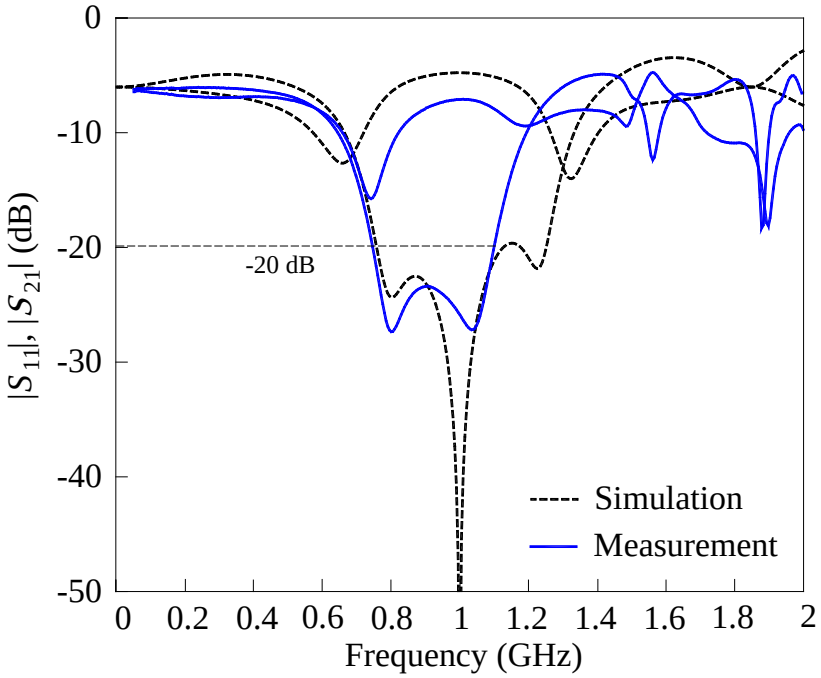
0
-10
-20
-30
-40
-50
-20 dB
Simulation
Measurement
0 0.2 0.4 0.6 0.8 1 1.2 1.4 1.6 1.8 2
Frequency (GHz)
|S11|, |S21| (dB)

(a)

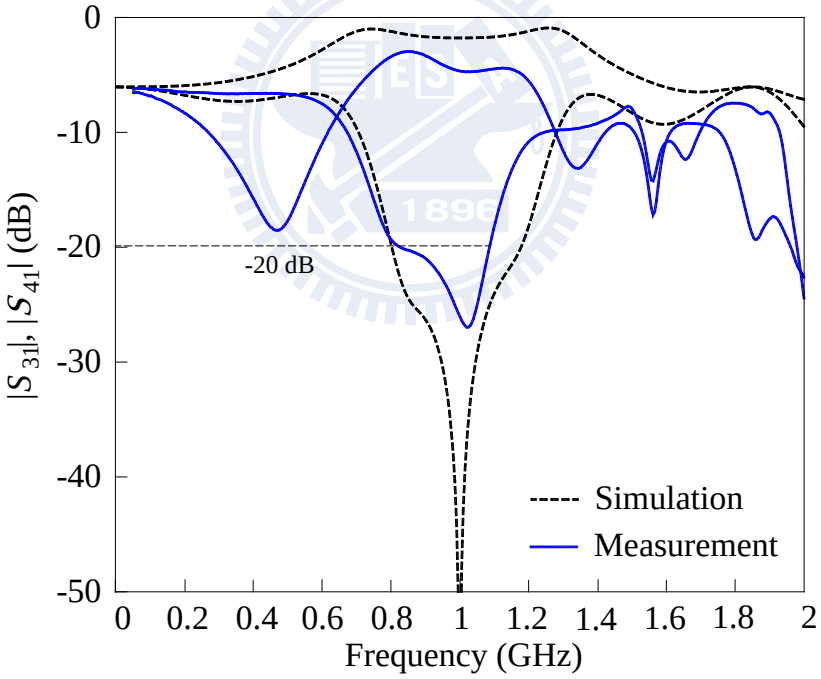
0
-10
-20
-30
-40
-50
-20 dB
Simulation
Measurement
0 0.2 0.4 0.6 0.8 1 1.2 1.4 1.6 1.8 2
Frequency (GHz)
|S31|, |S41| (dB)

(b)

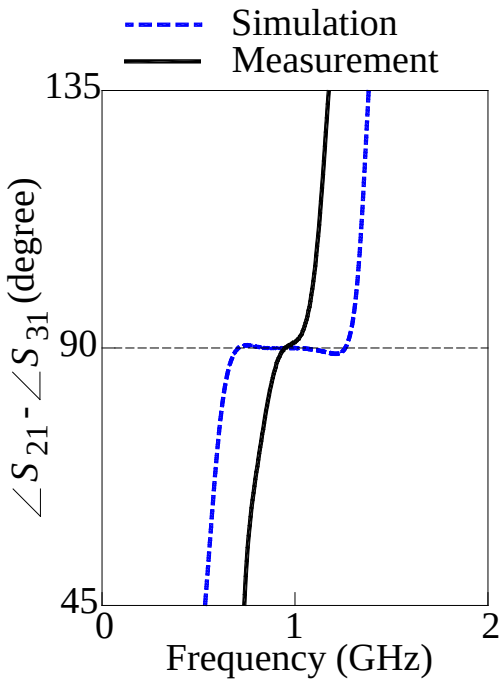

Fig. 3-8. Simulation and measurement of the 3-section branch-line coupler with -3dB power division. (a) $|S_{11}|$ and $|S_{21}|$ (b) $|S_{31}|$ and $|S_{41}|$ (c) The simulation and measurement of phase difference between S_{21} and S_{31}

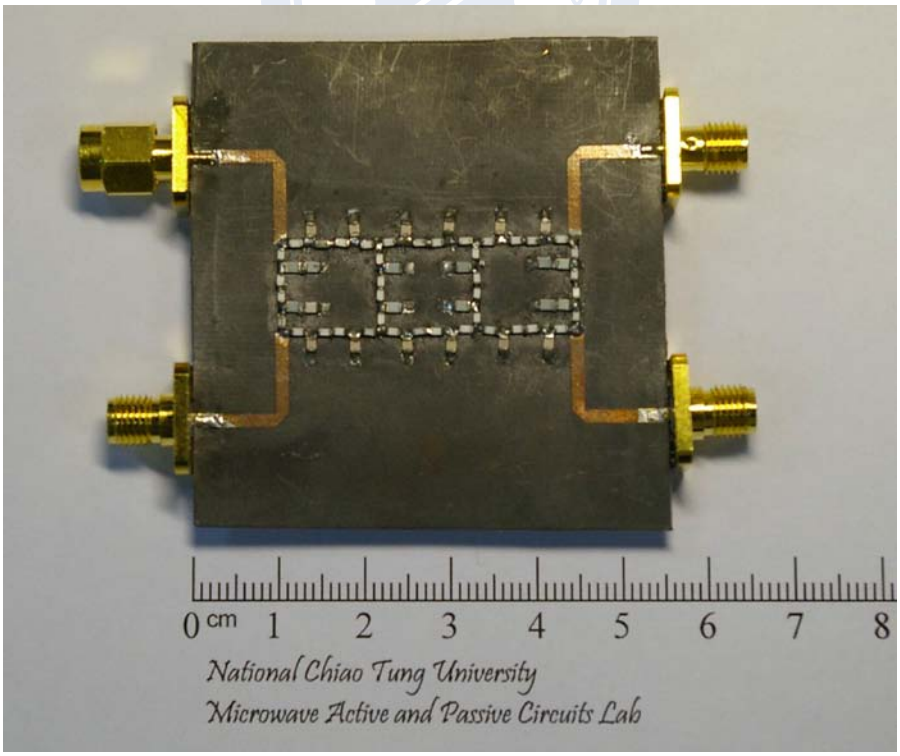

Fig. 3-9. The photo of Circuit 2

Table 3-5

Summary Data of the 3-Section Branch-Line Coupler with -3 dB Power Division

(Circuit 2)

	Simulation	Measurement
Operating frequency	1 GHz	1 GHz
Return Loss ($\|S_{11}\|$)	-66.47 dB	-25.87 dB
FBW*	42.44%	35.59%
Through ($\|S_{21}\|$)	-4.77 dB	-7.11 dB
Coupling ($\|S_{31}\|$)	-1.76 dB	-4.66 dB
Isolation ($\|S_{41}\|$)	-69.44 dB	-26.05 dB
FBW	37.94%	26.33%
$\angle S_{21} - \angle S_{31}$	90^0	90.57^0

* FBWs are in reference of -20 dB level.

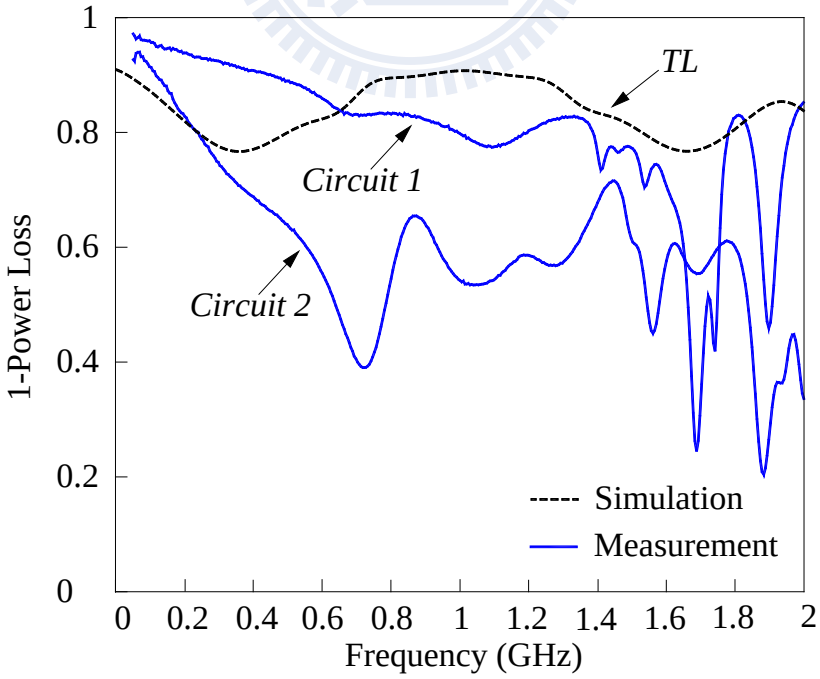

Fig. 3-10. Power loss of 3-section branch-line coupler with transmission lines, lumped distributed elements (Circuit 1), and all lumped elements (Circuit 2).

Fig. 3-10 plots the power losses for three fabricated circuits. $P_L = 1 - |S_{11}|^2 - |S_{21}|^2 - |S_{31}|^2 - |S_{41}|^2$ at operating frequency for three circuits are 9.3%, 20.2% and 45.8%, respectively. One can see that the power losses increase extremely while the frequency increases. As expected, the circuit with all lumped elements has a severe power loss due to dissipations caused by non-ideal lumped elements, solder and the via holes. This conclusion can be judged by observing that Circuit 1 has fewer capacitors and via holes than Circuit 2. Table 3-6 compares the detailed data for the three implementation approaches of 3-section branch-line coupler. Obviously, the circuit implemented by microstrip lines has good performances with comparatively low power loss, but costs a large area. The performances of the circuits implemented by lumped- and lumped distributed elements are inferior to the former one, but they can reduce the area greatly.

Table 3-6

Summary Data for 3 Types of 3-Section Branch-Line Couplers

	TL	Circuit 1	Circuit 2
Operating frequency	1 GHz	1 GHz	1 GHz
Return Loss ($\|S_{11}\|$)	-37.01 dB	-40.60 dB	-25.87 dB
FBW*	53.94%	33.15%	35.59%
Through ($\|S_{21}\|$)	-5.09 dB	-6.86 dB	-7.11 dB
Coupling ($\|S_{31}\|$)	-2.24 dB	-2.36 dB	-4.66 dB
Isolation ($\|S_{41}\|$)	-41.46 dB	-19.56 dB	-26.05 dB
FBW	39.94%	28.28%	26.33%
$\angle S_{21} - \angle S_{31}$	89.74^0	96.54^0	90.57^0
Circuit Area	9651.41 mm^2	2800 mm^2	653.34 mm^2
(mm^2)	(100%)	(29.11%)	(6.76%)
Power Loss	0.093	0.202	0.458

* FBWs are in reference of -20 dB level.

Chapter 4
Conclusion

Based on the principle of a branch-line coupler, an extended work has been presented in this thesis. Using cascading 3 section branch-line couplers, a wide fractional bandwidth design is reported. For arbitrary power division, the corresponding maximum fractional bandwidths are presented. The design curves also reveal that the more uneven power division, the narrower bandwidth the circuit has. Meanwhile, the large size problem due to utilizing transmission lines with quarter-wavelength can be tackled by replacing the transmission line sections with equivalent circuit models implemented by lumped elements or lumped-distributed elements. Yet, the power loss deteriorates the circuit performance while the amount of lumped elements is increased. The prototype circuits are simulated and fabricated to confirm the ideas. The sizes are reduced to 29.11% and 6.76% for the lumped distributed circuit and the lumped circuit. Also, the power losses are 20.2% and 45.8%, respectively. Measurement results are in good agreement with the simulations.

References

[1] J. Reed and G. J. Wheeler, “A method of analysis Of Symmetrical four-port net works,” *IRE Trans. Micro wave Theory and Techniques*, VOI. MT’T-4, pp. 246–252, October 1956.

[2] R. Levy and L. F. Lind, “Synthesis of symmetrical branch-guide directional couplers,” *IEEE Trans. Microwai,e Theory Tech.*, vol. MTT-10, pp. 80-89, 1968.

[3] M. Muracuchi, T. Yukitake, and Y. Naito, “Optimum design of 3-dB branch-line couplers using microstrip lines,” *IEEE Trans. Microw. Theory Tech.*, vol. MTT-31, no. 8, pp. 674–678, Aug. 1983.

[4] T. Hirota, A. Minakaw, and M. Muraguchi, “Reduced-size branch-line and rat-race hybrids for uniplanar MMIC’s,” *IEEE Trans. Microwave Theory Tech.*, vol. MTT-38, no. 3, pp. 270–275, Mar. 1990.

[5] I. Sakagami, M. Haga, and T. Munehiro, “Reduced branch-line coupler using eight two-step stubs,” IEE Proc -Microwaves Antennas Propag vol. 146 , 455–460, Dec. 1999

[6] Y.-H. Chun and J.-S. Hong, “Design of a compact broad-band branchline hybrid,” presented at the IEEE MTT-S Int. Microw. Symp. Dig., Long Beach, CA, Jun. 2005.

[7] Y.-H.Chun and J.-S.Hong, “Compact wide-band branch-line hybrids”, *IEEE Trans Microwave Theory Tech* vol. 54, NO.2, p.704–709, Feb. 2006

[8] C.-W. Tang and M.-G. Chen, “Synthesizing microstrip branch-line couplers with predetermined compact size and bandwidth,” IEEE Trans. Microw. Theory Tech., vol. 55, pp. 1926-1933, Sep. 2007.

[9] S. S. Liao, P. T. Sun, N. C. Chin, and J. T. Peng, “A novel compact-size branch-line coupler,” *IEEE Microw. Wireless Compon. Lett.*, vol. 15, no. 9, pp. 588–590, Sep. 2005.

[10] S. S. Liao and J. T. Peng, “Compact planar microstrip branch-line couplers using the quasi-lumped elements approach with nonsymmetrical and symmetrical T-shaped structure,” *IEEE Trans. Microw. Theory Tech.*, vol. 54, no. 9, pp. 3508–3514, Sep. 2006.

[11] K.W. Eccleston and S. M. Ong, “Compact planar microstripline branchline and rat-race couplers,” *IEEE Trans. Microwave Theory Tech.*, vol. 51, no. 10, pp. 2119–2125, Oct. 2003.

[12] C.T. Lin, C.L. Liao and C.H. Chen, “Finite-ground Coplanar-waveguide Branch-line Couplers,” *IEEE Microwave and Wireless Components Letters*, Vol. 11, No. 3, March 2001, pp. 127–129.

[13] T. N. Kuo, Y. S. Lin, C. H. Wang, and C. H. Chen, “A compact LTCC branch-line coupler using modified-T equivalent-circuit model for transmission line,” *IEEE Microw. Wireless Compon. Lett.*, vol. 16, no. 2, pp. 90–92, Feb. 2006.

[14] C.-W. Tang, M.-G. Chen, and C.-H. Tsai, “Miniaturization of Microstrip Branch-Line Coupler with Dual Transmission Lines”, *IEEE Microw. Wireless Compon. Lett.*, vol. 18, pp. 185-187, Mar. 2008.

[15] C.-W. Wang, T.-G. Ma, and C.-F. Yang, “Miniaturized Branch-Line Coupler with Harmonic Suppression for RFID Applications using Artificial Transmission Lines”, in *IEEE MTT-S Int. Microwave Symp. Dig.*, Jun. 2007,, pp.29-32.

[16] R. K. Gupta and W. J. Getsinger, “Quasi-lumped element 3- and 4-port networks for MIC and MMIC applications,” in *IEEE MTT-S Int. Microwave Symp. Dig.*, CA, 1984, pp. 409–411.

[17] R. W. Vogel, “Analysis and design of lumped- and lumped-distributed element directional couplers for MIC and MMIC applications,” *IEEE Trans. Microwave Theory Tech.*, vol. 40, pp. 253–262, Feb. 1992.

[18] I. Ohta, X.-P. Li, T. Kawai, and Y. Kokubo, “A design of lumped-element 3 dB

quadrature hybrids," in *Proc. Asia–Pacific Microwave Conf.*, 1997, pp. 1141–1144.

[19] Y.-C. Chiang and C.-Y. Chen, "Design of a wide-band lumped-element 3-dB quadrature coupler," *IEEE Trans. Microw. Theory Tech.*, vol. 49, no. 3, pp. 476–479, Mar. 2001.

[20] W. S. Tung, H. H. Wu, and Y. C. Chiang, "Design of microwave wide-band quadrature hybrid using planar transformer coupling method," *IEEE Trans. Microwave Theory Tech.*, vol. 51, no. 7, pp. 1852–1856, Jul. 2003.

[21] D. M. Polar, *Microwave Engineering*, 3rd ed. New York: Wiley, 2005, ch. 7.

[22] IE3D simulator, Zeland Software Inc., Jan. 2002.

[23] ADS, Aligent Technologies Inc., 2008

作者簡介

姓名：盧政良

性別：男

生出年月日：民國 74 年 5 月 28 日

籍貫：台北縣

學歷：

國立交通大學電信工程學系碩士班電波組	2007.7~2009.7
國立中央大學電機工程學系學士	2003.9~2007.6
國立板橋高級中學	2000.9~2003.6

碩士論文題目：以集總與分散式元件設計任意功率分配之旁枝耦合器